CHEMICAL REVIEWS

Review

Probing the Dynamics of Protein–Protein Interactions at Neuronal Contacts by Optical Imaging

Olivier Thoumine, Helge Ewers, Martin Heine, Laurent Groc, Renato Frischknecht, Grégory Giannone, Christel Poujol, Philippe Legros, Brahim Lounis, Laurent Cognet, and Daniel Choquet

Chem. Rev., **2008**, 108 (5), 1565-1587 • DOI: 10.1021/cr078204m • Publication Date (Web): 01 May 2008

Probing the Dynamics of Protein–Protein Interactions at Neuronal Contacts by Optical Imaging

Olivier Thoumine,*,† Helge Ewers,† Martin Heine,‡ Laurent Groc,† Renato Frischknecht,‡ Grégory Giannone,† Christel Poujol,§ Philippe Legros,§ Brahim Lounis,⊥ Laurent Cognet,⊥ and Daniel Choquet*,†

CNRS UMR 5091, Institut Magendie, Université Bordeaux 2, 33077 Bordeaux, France, Leibniz Institüt für Neurobiologie, Magdeburg, Germany, PICIN, Institut Magendie, Université Bordeaux 2, 33077 Bordeaux, France, and Centre de Physique Moléculaire Optique et Hertzienne, CNRS-Université Bordeaux 1, 33405 Talence, France

Received December 31, 2007

Contents

* Corresponding authors. E-mail: dchoquet@u-bordeaux2.fr; othoumin@u-bordeaux2.fr.
† CNRS UMR 5091, Institut Magendie, Université Bordeaux 2.
‡ Leibniz Institüt für Neurobiologie.
§ PICIN, Institut Magendie, Université Bordeaux 2.
⊥ Centre de Physique Moléculaire Optique et Hertzienne, CNRS-Université Bordeaux 1.

1. Introduction

In this review, we give an overview of the various optical-based methods allowing characterization of the assembly and turnover of macromolecular complexes present at neuronal contacts. We first briefly explain the biological paradigm and relevant molecular components. Then, we describe state of the art microscopy techniques that allow a dynamic visualization of specific elements at such contact sites. We focus sequentially on optical tweezers, FRAP, single-molecule and particle tracking, FCCS, and FRET/FLIM. Further, we outline in each case the mathematical analysis required to extract the physicochemical parameters that define protein–protein interactions. For illustration, we present recent data obtained in our laboratory as well as work from other groups, referring to a few specific examples. We conclude by comparing the pros and cons of these various approaches.

2. A Physicochemical Description of Neuronal Contacts

In the mammalian brain, 10^{11} neurons communicate via trillions of specialized cell contacts called synapses. Synapses are responsible for cognitive functions such as information processing, learning, memory, and motor control. To carry out these functions, synapses need to be (1) formed in a very precise manner during development, (2) well stabilized, and (3) highly plastic. To perform these in part contradictory tasks, the molecular machinery involved must be adaptive and highly dynamic, changing from adhesive to repulsive or from immobile to mobile depending on specific momentarily requirements. For example, transient contacts mediated by adhesion molecules play a crucial role during neuronal development. After a step of neuronal cell differentiation and migration that define specific brain areas, axons led by their growing tips, the growth cones, elongate and explore surrounding surfaces (Figure 1A). The interplay between adhesion and repulsion guides the growth cone along a predetermined pathway to target cells.[1] Also, during the process of synapse formation, cell−cell contacts between axonal filopodia and dendritic projections mediated by

10.1021/cr078204m CCC: $71.00
Published on Web 05/01/2008

Olivier Thoumine obtained an engineering degree from Ecole Centrale (Paris, France), at the end of which he was attracted to cell biology (Master's degree Paris VI, CEA Saclay). He moved to the U.S. and completed his Ph.D. in the lab of Bob Nerem at Georgia Tech (Atlanta), studying the adaptation of endothelial cells to fluid flow stimuli. He then did a post-doc at Institut Curie (Paris) in the physics group of A. Ott and J. Prost and stayed as an associate fellow at the Swiss Federal Institute in Lausanne (Switzerland) in the lab of J.J. Meister. He performed a number of studies dealing with cellular adhesion and mechanics. He obtained a tenure research position from the French academic system (CNRS) in 2001, in the team of Daniel Choquet (University Bordeaux 2). His research focuses on the role of adhesion proteins (N-cadherin, IgCAMs, neurexin/neuroligin) in growth cone migration and the establishment of early neuronal contacts.

Helge Ewers studied biochemistry at the University of Hannover, Germany, with thesis work in Neuroscience at the Mount Sinai School of Medicine in New York. In 2003, he moved on for a Ph.D. in cell biology with Ari Helenius at the ETH Zurich. His work there concerned membrane interactions of lipid-binding viruses. Since 2007, he has been a FEBS-Fellow in the laboratory of Daniel Choquet at the University of Bordeaux.

Martin Heine studied Biology at the Universities of Jena, Rostock (Germany) and Glasgow (Scotland). He obtained his Ph.D. in Zoology at the University of Göttingen (2002). He was awarded a post-doctoral fellowship from the German research community (DFG) to work in the group of Daniel Choquet at the University of Bordeaux (2002–2007). Since 2007, he has been a group leader at the Leibniz Institut for Neurobiology, Dept. of Neurochemistry (Prof. Gundelfinger). His research interests deal with synaptic plasticity and glutamate receptor/ion channel trafficking.

Laurent Groc is a Research Associate in Neuroscience for the French National Science Agency (CNRS, Bordeaux, France). He obtained his Ph.D. in cellular neuroscience at Wayne State University (Detroit, MI) and Université C. Bernard (Lyon, France). His interest in glutamatergic receptor trafficking started during his postdoctoral fellowship with Bengt Gustafsson and Eric Hanse in the Physiology Department of Göteborg University (Sweden). In 2003, he joined Daniel Choquet's group as a postdoctoral fellow to work on membrane diffusion, and a year later he was appointed Tenure CNRS Researcher. His research focuses on the interplay between receptor trafficking and neuronal connection refinements.

specific adhesion proteins (cadherins, IgCAMs, neurexin/neuroligin) represent one of the initial steps in the establishment of stable synaptic contacts (Figure 1B). Such transient adhesion is then stabilized to form a functional synapse through the recruitment of additional elements (cytoskeletal matrix, scaffolding proteins, functional receptor channels, . . .) both at the presynaptic and the postsynaptic site, in a precisely ordered sequence[2,3] (Figure 1C).

Apart from very specialized structures such as the giant mossy fiber terminals in the hippocampus or the neuromuscular junction (NMJ), most mature synapses in the central nervous system (CNS) have a small diameter (300–500 nm) and two highly specialized pre- and postsynaptic compartments facing each other and separated by a narrow space (30 nm), the synaptic cleft. The presynaptic terminal contains a cytomatrix, which is thought to coordinate the high number of synaptic vesicles filled with neurotransmitters (i.e., glutamate in the case of excitatory synapses, glycine or GABA for inhibitory synapses). Arrival of an action potential (a wave of membrane depolarization propagating through the axon) to the presynaptic terminal leads to a rise in the intracellular concentration of bivalent calcium ions and, subsequently, to fusion of synaptic vesicles with the plasma membrane at the active zone to release their neurotransmitter content into the synaptic cleft.[4]

The most prominent feature of the postsynapse is the electron-dense intracellular material visible in electron microscopy at excitatory synapses. This structure, termed the *postsynaptic density*, contains a large number of scaffolding proteins that stabilize the different subtypes of glutamate receptors at the plasma membrane.[5,6] Binding of the presynaptically released transmitter to ionotropic receptors induces the opening of those ion channels and subsequently, depending on the type of

Renato Frishknecht completed his undergraduate studies in biochemistry at the University of Zurich (Switzerland) and then completed a Ph.D. thesis at the Biochemical Institute also at the University of Zurich (1999–2005). He was awarded a fellowship from the Swiss National Fund to work as a post-doctoral fellow at the Leibniz Institute for neurobiology in Magdeburg (Germany), in the group of Eckart Gundelfinger, where he has been since 2005. His research focuses on biochemical characterization of the molecular interactions with extracellular matrix components involved in modulating synaptic transmission.

Grégory Giannone received his Ph.D. in cell biology at the Louis Pasteur University in Strasbourg (France) in 2001. The main focus of his research, including postdoctoral studies in the laboratory of Michael Sheetz at Columbia University in New York City, was the temporal and spatial dynamics of structures involved in cell motility. In 2005 he obtained an assistant professorship at the CNRS in France and joined the laboratory of Daniel Choquet. His current research interests include the temporal and spatial dynamics and organization of proteins and proteins complexes involved in cell motility and initiation of synaptic contacts, using single protein tracking techniques.

Christel Poujol completed her Ph.D. in cell biology at the University of Bordeaux 2 (France) working on platelet-related diseases using transgenic models and electron microscopy. She spent three years on the CNRS campus at Gif/Yvette (France), working as an engineer in a bio-imaging facility. She joined the Imaging Center (PICIN) at Bordeaux 2 in 2004. She is responsible for training users in confocal and video microscopy, and she is involved in several projects using FRET/FLIM techniques.

Philippe Legros completed a bachelor's in astrophysics in Toulouse (France) and a Master's in optics instrumentation (Saint Etienne, France). He spent three years as a physics engineer at the European Center for Nuclear Research (CERN, Geneva, Switzerland) working with high power lasers. In 2002, he obtained an engineer position from CNRS at the University of Bordeaux, and worked with Daniel Choquet in setting up the bio-imaging facility. He is now in charge of developing new optical imaging technologies based on femto-second lasers.

receptors, to a change in the local membrane potential of the postsynaptic neuron (Figure 1C). One important feature of synapses is indeed their adaptability. Upon specific electrical stimulations (which can be mimicked by chemical protocols), synapses can either be potentiated or depressed, resulting in higher or lower efficacy of synaptic transmission, respectively. These effects are induced rapidly, i.e., in seconds, and can be long lasting, i.e., hours to days or even longer. They are thought to represent the basis for memory coding and are associated with changes in synapse morphology and numbers of postsynaptic functional receptors.[7] Thus, synapses are dynamic objects mediating a dialogue between pre- and postsynaptic neurons, and synaptic specificity and plasticity are governed by a complex set of molecular interactions.

Although synapses can last for years,[8] recent observations based on time-lapse imaging of fluorescently labeled proteins have revealed that individual molecular elements turn over rapidly.[9–12] From a physicochemical perspective, an interesting problem lies in the maintenance of a locally stable architecture, based on labile interactions. The precise measurements of the actual numbers of proteins present in synaptic compartments, as well as on rates and off rates of the various molecular interactions involved, might help understand how this is achieved. Among the relevant parameters are the surface density of molecules, the diffusion coefficient within the membrane plane, the fluxes between cytosol and membranes by endocytosis and exocytosis, and the individual protein–protein reaction rates (Figure 2). Given the relatively small size of synapses, only a small number of well-identified proteins are involved in these interactions (see next paragraph). Thus, a deterministic framework based on average concentrations is no longer valid, and a probabilistic description is needed that considers stochastic fluctuations in the numbers of interacting molecules.[13] Such models can demonstrate the metastability of small synaptic clusters, corresponding to conditions of synaptic plasticity.[14] In the following sections, we review

Brahim Lounis obtained a Ph.D. in laser cooling and trapping of atoms at ENS (Paris) in the group C. Cohen-Tannoudji. He was appointed assistant professor at Bordeaux University in 1993, where he performed pioneering studies on quantum optics with single molecule and developed the first single photon sources. After a sabbatical at Stanford University, he became a Professor at Bordeaux University, where he leads the Nanophotonics group. His research interests concern Nano-Optics. He develops new optical methods for detection and study of individual nano-objects and studies their applications in quantum optics and in neurobiology.

Laurent Cognet is Research Associate in Physics for the French National Science Agency (CNRS). After his education as an optics engineer at École Supérieure d'Optique (Orsay, France) and a Ph.D. in atom optics supervised by A. Aspect (Institut d'Optique, Paris-Sud University), he joined Th. Schmidt (Leiden University, NL) for a postdoctoral fellowship to focus on the optical detection of individual biomolecules in live specimens. In 2000, he was appointed Tenure Researcher by CNRS in the Nanophotonics group headed by B. Lounis at Bordeaux University. His main interests deal with the development of the optical detection of individual nano-objects, their spectroscopy and their applications in neurobiology. For this work, he was awarded CNRS Bronze medal in 2005. In 2006–2007, he obtained a Fulbright Research Award to spend a sabbatical year at Rice University with R.B. Weisman, where he extended the use of single-molecule spectroscopy on single-walled carbon nanotubes.

the optical techniques that are currently developed to explore such molecular dynamic within a small compartment like a synapse.

3. Counting the Number of Molecules at Neuronal Contacts

3.1. Nonoptical Methods

Before measuring interaction rates between proteins, it is desirable to have an estimate of the numbers of interacting species within the cellular compartments of interest (plasma membrane, intracellular vesicles). This is not a trivial issue, and several methodologies have to be used in parallel to

Daniel Choquet obtained an engineering degree from Ecole Centrale (Paris, France), at the end of which he was attracted to neuroscience (Master's degree Paris VI). He completed his Ph.D. in the lab of H. Korn at the Pasteur Institute (Paris), studying ion channels in lymphocytes. He was appointed Tenure Research officer at the CNRS in 1988 in the group of Korn. He then did a post-doc/sabbatical at Duke University (North Carolina) in the laboratory of Michael Sheetz where he studied the regulation of integrin-cytoskeletal linkages by mechanical force. He then set up his group in Bordeaux and got a directorship position at the CNRS. He launched an interdisciplinary program on the use of high resolution imaging to study the trafficking of neurotransmitter receptors in neural cells. He is now heading both his research group and the Bordeaux imaging core facility, and he is developing several research subjects combining neuroscience, physics, and chemistry to unravel the dynamics of multimolecular complexes and their role in synaptic transmission. He's been the recipient of several awards including the 1990 Bronze medal from the CNRS, the Research prize from the Foundation pour la Recherche Médicale (1997) and the grand prix from the French Academy of Sciences, prix du CEA.

validate the measurements. A first approach is based on *biochemistry and proteomics*. Mass spectrometry analysis of "synaptosomes" obtained from brain extracts has allowed the identification of the major components of pre- and postsynapses.[15–18] It is *a priori* possible to estimate the number of copies of each protein per synapse by running the sample against known quantities of purified proteins and dividing by the number of synaptosomes measured independently. Another approach involves electron microscopy and a newly developed *immunogold labeling technique* using detergent-digested freeze-fracture replica. This has allowed a precise visualization of individual endogenous glutamate receptor clusters in the postsynaptic membrane with nanometer resolution[19] and gives an average value of 80 AMPA receptors per synapse, corresponding to surface densities on the order of 400–2400 μm^{-2} (depending on synapse type). Another approach uses *electrophysiology*. It is based on patch-clamp recordings of currents elicited by local iontophoretic glutamate delivery at synaptic boutons in primary cultures[20] or by miniature quantal release of presynaptic vesicles in brain slices.[21] By estimating the charge carried by a single glutamate receptor channel, one can calculate the minimum surface density of AMPA and NMDA receptors, whose respective contribution can be isolated by specific antagonists. This method yields density estimates on the order of 10^4 μm^{-2}, corresponding to approximately 400 receptors of each type per synapse, and only 3 μm^{-2} in the extrasynaptic membrane.[20]

3.2. Optical-Based Methods

A more recent approach involves the *optical detection of fluorescent proteins* in neurons. Since the discovery of the

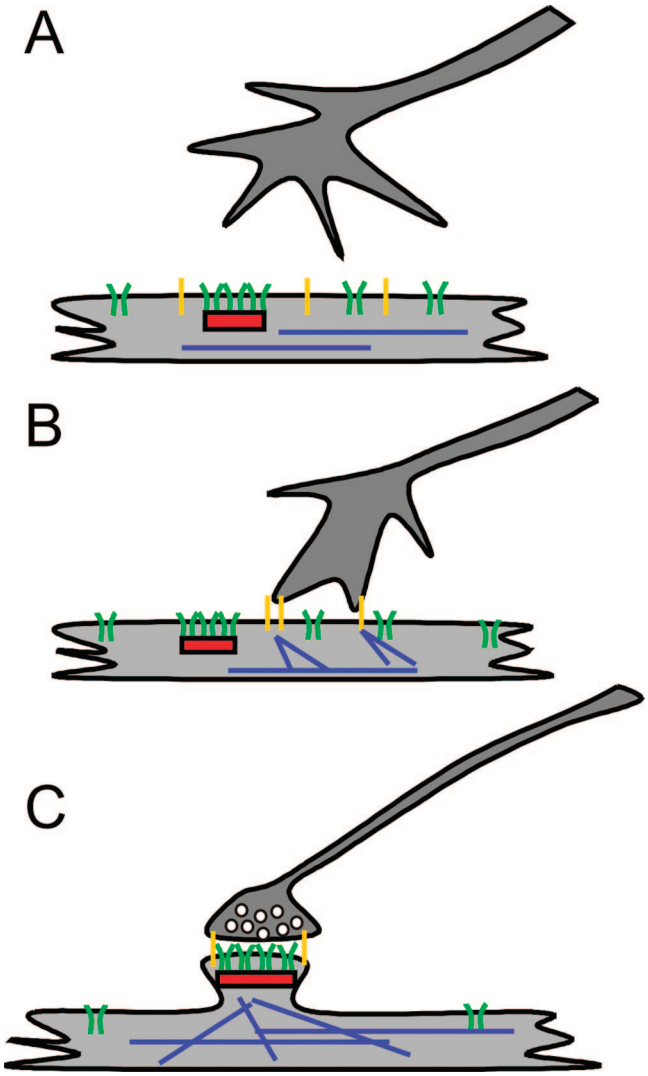

Figure 1. The making of a synapse. (A) Growth cones are motile structures at the extremity of axons, which migrate through the nervous tissue, guided by soluble factors and adhesion proteins. (B) Initial contact between axonal filopodia and dendrites of a target cell, mediated by interactions between adhesion proteins (yellow) and stabilized by the cytoskeletal network (blue lines). (C) Contact maturation, recruitment of scaffolding proteins (red) and neurotransmitter receptors (green), which will form the postsynaptic density. The presynapse is a dense cytomatrix filled with vesicles rich in neurotransmitters.

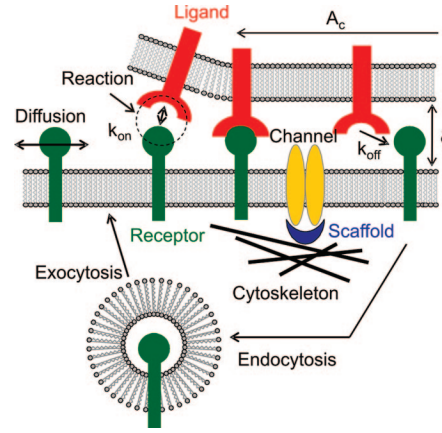

Figure 2. Molecular scale view of a cell−cell contact. The relevant parameters controlling the presence of macromolecular assembly at the adhesive interface between two cells are shown: receptor diffusion at the plasma membrane, stabilization through interactions with *trans*-binding counter-receptors in the opposite plasma membrane (for adhesion proteins) or scaffolding components (for neurotransmitter receptor channels), and exchanges (fluxes) between vesicular compartments and the plasma membrane through exo- and endocytosis of vesicles, respectively. The cytoskeleton provides a dynamic anchor to both adhesion proteins and scaffold proteins. The making of an adhesive bond involves receptor diffusion to the vicinity of a ligand (an encounter diameter is outlined), followed by the reaction step itself (k_{on}). Ligand–receptor bond lifetime at the contact is characterized by k_{off}. The adhesive zone is shown as area A_c and separation distance by δ.

green fluorescent protein (GFP) from jellyfish in 1978,[22] the specific detection of proteins in live cells is possible with the high signal-to-noise ratio of fluorescence.[23] This is achieved by fusing the coding sequence of the protein of interest to the coding sequence of the green fluorescent protein, resulting in a single polypeptide chain when expressed in live cells. The translated protein bears a fluorescent tag that allows its precise localization and quantitative measurements of single-molecule and ensemble fluorescence. To date, over 20 different isoforms and analogues of GFP have been discovered and engineered to cover the entire visible spectrum,[24] so that simultaneous detection of differentially tagged proteins is possible in live cells.[25] The structure of several GFP isoforms is solved at atomic resolution, and the photophysics of FPs and their respective fluorophores is the object of intense investigation.[26] Furthermore several GFPs have been engineered as sensors for specific intracellular environments such as pH[27] and redox-state,[28] or to intentionally yield high phototoxicity to damage specific cells or organelles.[29] The pH-dependent GFP, pHluorin, has proven to be particularly useful to investigate bulk and specific membrane protein turnover, since its fluorescence is quenched in the intravesicular acidified environment of the endocytic pathway. Another important newly developed tool is the photoswitchable FPs, which are nonfluorescent unless activated by a brief pulse of UV light.[30,31] By specifically activating small localized protein populations, the fate of this population can be followed in live cells over time.[32,33]

The genetically engineered fusion-proteins can be expressed in neurons under the control of appropriate promoters via transfection of bacterial vectors containing the engineered DNA. Several methods for cellular delivery are established.[34] Commercial kits are available for *in vitro* transfection of cultured neurons by a liposome-based mechanism, but precipitating the DNA onto cells by the use of calcium phosphate is also efficient.[35] Unfortunately, the expression levels from most widely used plasmids are not well controlled and the efficiency of neuronal delivery decreases with time in culture. Genetically modified viruses that carry the coding sequence for the fluorescent fusion-protein in their genome provide a more sophisticated solution. An even more elegant, but labor-intensive, approach is the genetic engineering of mice to incorporate the desired sequence into their genome for expression in specific brain regions.

To quantify the number of proteins in subcellular compartments using GFP fusion-proteins, the first step is to estimate the level of overexpression of the engineered protein in comparison to the endogenous molecule: this can be quantified by immunocytochemistry. The second step is to compare the fluorescence intensity obtained in given compartments (a single synapse, an exocytic vesicle) to calibration standards, for example the signal of a single GFP molecule,[36] a known number of GFP molecules,[37] or fluorescent micro-

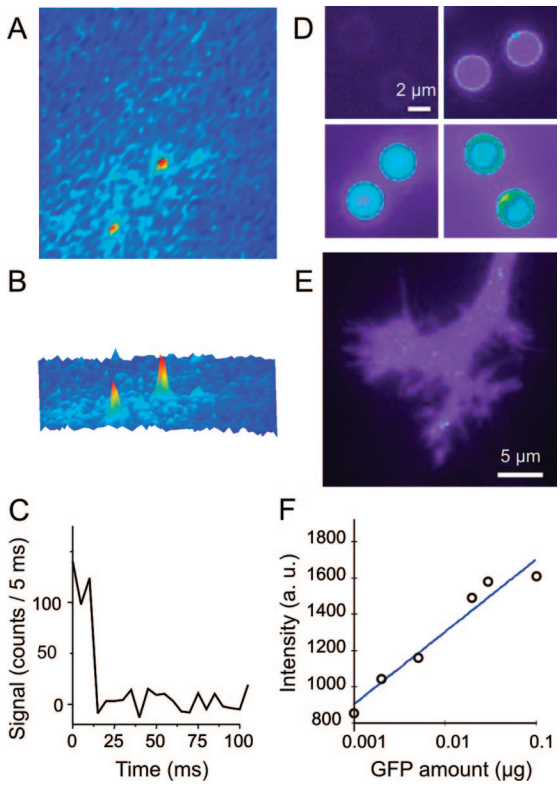

Figure 3. Counting proteins at the cell surface. (A) Single-molecule fluorescence detection of mGluR5-eYFP in the plasma membrane of COS-7 cells and (B) 3D plot of the fluorescent signal obtained from it. (C) Fluorescence intensity versus time trace of a single eYFP-mGluR5 molecule showing rapid one-step photobleaching. The sample was excited with 514 nm laser light for 5 ms/point at 4 kW/cm^2. (D) Microspheres were coated with a secondary antibody (goat anti-rabbit Fc), then with a primary rabbit antibody against GFP, and finally with various amounts of purified GFP to establish a ruler (100–10 000 molecules/μm^2). Beads were adsorbed on poly lysine coated glass and immuno-stained with cy3-conjugated anti-GFP in parallel with neuronal cultures transfected with an adhesion protein (NrCAM) fused with GFP (E). (F) Comparison of the signal from the transfected cells with the standards allows quantification of the surface density of expressed NrCAM molecules.

spheres previously calibrated against single GFP molecules.[38] Using this quantitative approach, estimates of about 200–300 PSD-95 molecules in a single synapse and 50 AMPA receptors delivered by a single exocytic vesicle have been obtained. The idea to count molecular assemblies using autofluorescent proteins arose simultaneously with the first observations of single GFPs in living cells.[39,40] The formation of cadherin oligomers was identified in the plasma membrane through the observation of well-defined peaks in the fluorescence intensity of tagged GFP molecules.[39] A similar strategy was used to measure the aggregation of L-type Ca^{2+} channels on dynamic clusters[41] or to count the number of GFP-tagged subunits in single receptors. An important limitation of this approach is that the photophysics of autofluorescent proteins is not favorable for single-molecule measurements[40] and is dependent on the local environment (in particular pH and membrane lipids), which is likely to be different in real cells and in calibration samples. In particular, rapid photobleaching of single molecules renders such quantifications difficult (Figure 3A−C). More subtle difficulties involve the quenching of fluorescence and possibly homo-FRET (see section 9.1) that can occur when several GFP molecules occupy a restricted space, resulting in an underestimation of the number of molecules present.

We recently circumvented the problem of photobleaching by proposing a single-molecule approach for counting autofluorescent proteins. We tested the method using a molecular scale consisting of individual citrin (a yellow GFP isoform) oligomers made by fusion of individual citrin molecules with tenascin arms, which form coiled-coils.[42,43] The method relies on the measurement of the total intensity emitted by each multimer until it photobleaches. This strategy overcomes the inherent problem of blinking and bleaching of GFPs. In the case of small protein aggregates, it allows precisely describing the mean composition with a precision of one protein. It does not however eliminate the problem of homo-FRET. In a similar approach, by counting individual bleaching steps of GFP fused to membrane receptors, the composition of multisubunit receptor channels such as NMDA receptors could be determined.[44] To determine bulk surface densities of molecules on cell membranes, another possibility is to use microspheres coated with small numbers of GFP molecules, but to perform additional immunocytochemistry instead of using the intrinsic GFP fluorescence signal. The use of antibodies to stain GFP under the same conditions for both the cells and the calibration standards will reduce the problems linked to GFP fluorescence. The number of GFP molecules bound to the beads can be measured independently by quantitative Western blotting, using known amounts of purified GFP. An example of this approach is given in Figure 3D−F, allowing quantification of the surface density of GFP-tagged IgCAM adhesion molecules on a growth cone surface, on the order of 1000 μm^{-2}.

4. Measuring Association Rates between Neuronal Adhesion Proteins

4.1. Definition and Properties of k_{on}

During axonal elongation, transient contacts are made between growth cones and the extracellular matrix or surrounding cells, as well as more stable contacts between axons that will make nerve fibers (i.e., fasciculation). When two cells contact each other, they can form selective and durable bonds mediated by specific adhesion proteins at the plasma membrane. These usually utilize key−lock structural interfaces involving specific amino acids and mediated by a combination of electrostatic and hydrophobic interactions (Figure 2). There exist several superfamilies of cell adhesion molecules (CAMs), including immunoglobulins, integrins, cadherins, selectins, neurexins/neuroligins, and ephrins. In the central nervous system, many of these proteins are expressed with precise developmental profiles and serve different functions. For example, immunoglobulin cell adhesion molecules (IgCAMs) are involved in axon fasciculation and outgrowth; synCAMs and neurexin/neuroligin, in synaptogenesis; and N-cadherins, in cell positioning and dendritic branching.[45–47] Most of the CAMS present at synapses are involved in synaptic plasticity.[48] Genetic mutations in some proteins responsible for growth cone navigation (L1) and synaptogenesis (neuroligins) are linked to brain disorders including certain forms of mental retardation[49] and autism,[50–52] respectively, demonstrating the clinical importance of these processes.

Although these proteins are linked to different signaling pathways, they share a common property, which is to bind to a specific counter-receptor on the surface of the adjacent cell. The formation and maintenance of initial cell−cell

contacts relies on the individual kinetic properties of the molecular bonds between CAMs. Many recent studies have addressed the issue of bond formation between biological molecules at cell surfaces,[53] using techniques such as atomic force microscopy,[54,55] micropipette manipulation,[56] the bioprobe force apparatus,[57] the laminar flow chamber,[58] centrifugation,[59] and optical tweezers.[60,61] The general aim of these approaches is to resolve single-molecule interactions. Thus, one has to use very dilute receptor and ligand coating concentrations and quick contact times to ensure that bonds are indeed mediated by a single ligand–receptor pair.[62]

The interaction between a receptor R and a ligand L expressed at cell surfaces can be described by a simple chemical reaction:

$$R + L \leftrightarrow R{\cdot}L$$

Here, the formation of the molecular complex R·L is characterized by an association rate k_{on} and a dissociation rate k_{off}. Because the two molecular species are membrane associated, they are expressed in units of surface density (#/μm^2). The forward rate constant k_{on} is then in units of $\mu m^2/s$ and the reverse rate constant k_{off} in s^{-1}. The consensus is that, in two dimensions, k_{on} is a complex parameter that depends first on translational and rotational diffusion, which allow the two molecules to achieve sufficient proximity and proper orientation, respectively.[63,64] k_{on} is also sensitive to the separation distance between the two surfaces (δ), which can be quite variable if the surfaces are rough. Therefore, the on rate is often combined with the contact area A_c, which is difficult to measure accurately, to yield a lumped parameter $k_{on}{*}A_c$ in units of $\mu m^4\ s^{-1}$.[65] For example, the presence of a first bond that brings the two surfaces in close proximity increases the chances of forming a second bond and so on.[66] The compressive force that reduces the potential repulsive barrier between the two cells and thus increases the effective contact area also affects k_{on}.[60] The interaction between the two molecules may show several binding states, linked to the specific structural interfaces formed between the molecules, as was elegantly demonstrated for cadherins.[67,68] More surprisingly, the outcome of a ligand–receptor interaction was also found to depend, either positively or negatively, on the previous adhesion event, in a "memory-like" type of coding.[69] Based on such single-molecule measurements, an important issue is to understand how individual properties determine the behavior and fate of a collective assembly of adhesion receptors in a natural cell−cell contact.

4.2. Measurement of 2D Affinity

Another relevant parameter to characterize adhesive cellular contacts is the equilibrium 2D dissociation constant $K_d = [R][L]/[R{\cdot}L]$, where [R·L], [R], and [L] are the densities of bound receptor–ligand complex, free receptor, and free ligand, respectively, in the contact area. The quantities [R] and [L] can be determined independently, e.g., by radioactive counting of isotope-labeled molecules or as described above (section 3.2). By definition, K_d is also equal to the ratio k_{off}/k_{on}. By writing $[R]_t$, the density of total receptors, the conservation of receptor number in the contact area can be formulated as

$$[R] = [R]_t - [R{\cdot}L] \quad (1)$$

This equation can be written in Scatchard form, i.e., by expressing bound/free ligand versus bound ligand, as

$$[R{\cdot}L]/[L] = [R]_t / K_d - [R{\cdot}L]/K_d \quad (2)$$

K_d can then be estimated from the negative slope of this relation, after quantifying the kinetics of bond accumulation, which can be done for example by observing the accumulation of fluorescent receptors at the contact (see section 4.3). This analysis relies on the hypothesis that the total receptor density $[R]_t$ is constant over the cell surface, but if the receptors are freely mobile within the bilayer, this approximation is no longer valid: $[R]_t$ depends in fact on free ligand density, and one has to refine the model accordingly.[70] K_d values in 2D contacts have been successfully measured for molecules implicated in the formation of the *immunological synapse*, which represents the adhesive interface between T lymphocytes and antigen presenting and target cells, and is involved in T cell activation.[65] For example, the interaction between immunological cell adhesion molecules CD2 and LFA-3 has a K_d on the order of 20 molecules/μm^2, and that of CD2-CD58 is 6 molecules/μm^2, usually lower than the 3D values, suggesting that the 2D environment promotes adhesion strengthening.[71] The use of artificially assembled bioactive surfaces such as supported lipid bilayers that contain mobile or immobile ligands to cell surface receptors has proven to be quite powerful in this area. With this assay, adhesive interactions cooperate so as to generate ideal membrane alignment with nanometer precision.[72] The extracellular domains of adhesion proteins can be artificially anchored to the lipid bilayer via glycosylphosphatidylinositol (GPI) groups and display free 2D diffusion in the plane of the membrane, which can be assessed by FRAP[73] (see section 5). If a cell is brought into contact with such a surface, the dynamics of the cellular response to ligand presentation can be studied under controlled conditions with fluorescence microscopy. For example, T cell receptor ligands initially engaged in an outermost ring of the nascent synapse are gradually transported into the central cluster, depending on T cell receptor ligand interaction kinetics.[74] A theoretical framework has been proposed to account for immunological synapse assembly, based on a set of differential equations to describe membrane-constrained protein-binding interactions.[75,76]

A major advantage of this experimental system is that it allows the use of high spatial resolution provided by *total internal reflection fluorescence* (TIRF) microscopy.[77] This technique is based on the use of a laser beam focused on the back focal plane of a high numerical aperture objective and coming at an angle above the refraction limit at the cell−substrate interface.[78] Total reflection of the laser is accompanied by the propagation of an evanescent wave whose intensity decreases exponentially with distance on a characteristic scale around 100 nm, which limits the fluorescence illumination to a narrow optical section at the substrate interface. One can then focus on the regions of interaction between cells and the coated substratum and increase the signal-to-noise ratio. For example, the spatial arrangement and dynamic assembly of protein–protein complexes and steady-state shift of protein–protein interactions in T cell signaling have recently been demonstrated at the single-molecule level using TIRF.[79]

However, application of this approach to the assembly of neuronal synapses, which are much smaller and contain far more components on both sides of the synaptic cleft, will be difficult (for a comparison of neuronal and immunological synapses, see ref 80). Initial studies with heterologous cells

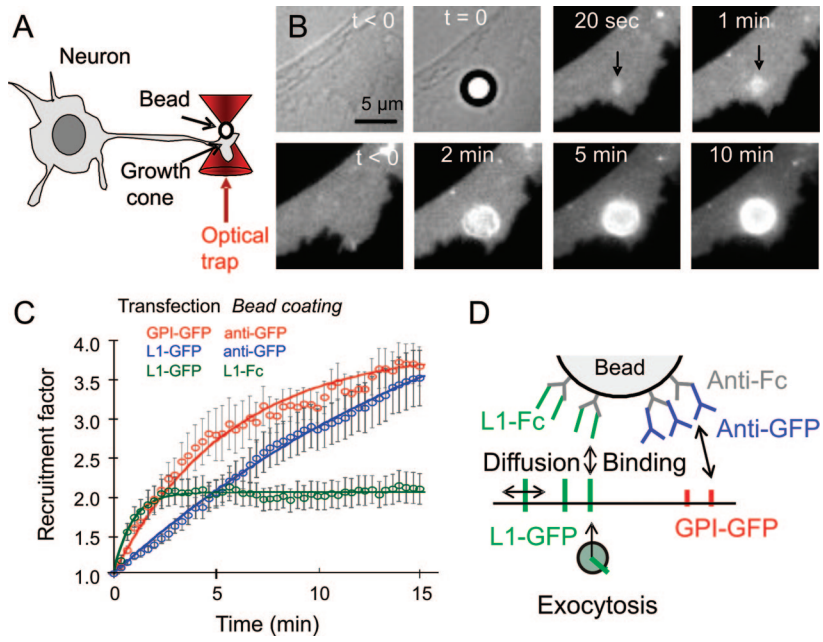

Figure 4. Effects of membrane diffusion and local exocytosis on the rate of receptor accumulation. (A) Schematic of the optical tweezers experiment. (B) Example of recruitment of an NrCAM construct bearing an extracellular GFP tag, by a microsphere coated with antibodies against GFP. (C) Three examples of receptor recruitment kinetics. The fluorescence at the bead contact is normalized by that on a control region. The average of more than 10 individual beads is presented for the three situations depicted in (D). In red, GFP anchored to the upper membrane leaflet by a glycosyl-phosphatidyl-inositol (GPI) group, thus displaying fast diffusion, is recruited quickly by anti-GFP-coated beads. In blue, full-length L1-GFP showing reduced membrane mobility is recruited more slowly by anti-GFP-coated beads. In green, L1-GFP is recruited very fast by L1-Fc-coated beads, owing to the contribution of local exocytosis.

and supported membrane bilayers using the neurexin−neuroligin interaction,[81,82] which is known to be involved in synapse formation,[83] have demonstrated the general feasibility of such an approach for neuronal synapses.[84] One difficulty of these assays lies in the absence of control of the initial time point of the adhesive interaction. Microspheres coated with lipids and GPI-anchored neuroligin, which have been shown to trigger presynaptic differentiation on axons of primary neurons,[85] in combination with optical tweezers, could help solve this problem (see below).

4.3. Measuring k_{on} Using Optical Tweezers and Time-Lapse Fluorescence Microscopy

Here we provide examples of how *optical tweezers* in combination with time-lapse fluorescence imaging can be used to probe the association rates between adhesion proteins in living neurons. Optical tweezers consist of a parallel laser beam brought into focus by a high numerical aperture microscope objective. The convergent rays of light behave as a three-dimensional trap for dielectric particles such as latex or glass microspheres.[86] Since laser powers up to 100 mW can be necessary for efficient trapping, the wavelength is chosen in the near-infrared, a spectral region where biological samples absorb little light, in order to avoid photodamage. Thus, optical trapping can be superimposed to fluorescence imaging using appropriate dual dichroic mirrors. Microspheres can be coated with specific antibodies or ligands, such as the outer domains of adhesion proteins fused to the constant fragment of human IgG and produced as recombinant proteins. These constructs, coated onto a layer of anti-Fc antibodies adsorbed on the microspheres, allow a proper orientation and functionality of the adhesive moieties. Microspheres are brought into contact with the region of interest, e.g., the dorsal surface of a neuronal growth cone or a neurite. In these experiments, the optical trap is used essentially to control the time zero of the adhesive interaction. The position of the microsphere is tracked in the transmitted light channel, and the redistribution of GFP-tagged molecules transfected into the neuron is followed in the epifluorescence channel. One can thus observe a progressive accumulation of adhesion receptors at microsphere contacts and quantify its kinetics, starting from the initial contact (Figure 4).

Using first-order kinetics as before, the surface density of receptor–ligand complexes (R•L), noted C, is given by:

$$d[C]/dt = k_{on}[R][L] - k_{off}[C] \quad (3)$$

where [R] and [L] are the free receptor and ligand densities at the cell and bead surfaces, respectively. The pool of surface receptors is sufficiently large when compared to the bead area, so we can neglect receptor depletion and set $[R] = [R]_t - [C] \cong [R]_t$. Given the initial condition of no bond, the solution of this differential equation is

$$[C(t)] = [C]_\infty[1 - \exp(-kt)] \quad (4)$$

with two pooled parameters $k = k_{on}[R]_t + k_{off}$, which represents an overall rate constant, and $[C]_\infty = [L]/(1 + k_{off}/k_{on}[R]_t)$, which is the steady-state bond density. In the case of antibody–antigen interactions, which are very stable, we can set $k_{off} = 0$, and the steady state corresponds to saturation of ligand sites on the microspheres. The fluorescence level around beads is normalized by a control level on a nearby region, allowing reduction of potential photobleaching effects, and the data are fitted by the expression $1 + [C(t)]/[R]_t$. The measurements of [L] and $[R]_t$ by independent biochemistry and immunocytochemistry experiments allow us to compute the intrinsic rates k_{on} and k_{off}.

Using this method, we have studied various ligands or antibodies and corresponding adhesion receptors, i.e., cadherins and IgCAMs.[87–89] In a recent study, we questioned whether the regulated interactions of IgCAMs receptors to a static actin cytoskeleton in growth cones, e.g., through ankyrin and ERM proteins,[90,91] could affect the rate of adhesion formation by reducing the diffusiveness of IgCAMs on the cell surface.[87] Using various truncations in the extra- and intracellular domains, we could modulate the lateral mobility of GFP-tagged IgCAMs. This translated into modest but significant effects on the rates of receptor accumulation at anti-GFP-coated microspheres. For example, the NrCAM transmembrane domain fused with GFP diffuses 5 times more rapidly than the full-length L1 molecule and shows a 2-fold higher on-rate (Figure 4C). This agrees with the basic concept that adhesion is composed of two steps: (1) receptor diffusion to the vicinity of its ligand and (2) receptor–ligand interaction *per se*.[63,64]

Another observation is related to the active recycling of L1 within growth cones. By interacting with the clathrin adaptor AP-2 through a specific motif in its intracellular tail, L1 can undergo endocytosis in the central domain and exocytosis at the periphery of the growth cone.[92] This mechanism generates a density gradient of L1 molecules, which helps growth cones to progress forward.[45] We showed that L1-GFP accumulated faster at microspheres coated with L1-Fc proteins than at antibody-coated beads, indicating either faster reactivity and/or additional processes. The use of an L1-GFP construct in which the N-terminal GFP could be cleaved off rapidly by thrombin allowed the identification of newly exocytosed L1-GFP molecules.[89] L1-GFP still accumulated at L1-Fc microspheres after thrombin treatment, indicating that local exocytosis of L1-rich vesicles at the growth cone participates in enhancing the formation of L1 homophilic contacts.[89] These effects were specifically triggered by L1−L1 adhesion since they were not observed for beads coated with antibodies and the exocytosis rate of L1 was much higher than in the absence of beads. Rapid saturation in the level of L1 molecules at L1-Fc microspheres was interpreted by the fact that L1−L1 bonds can also undergo rapid dissociation (nonzero k_{off}), so the steady-state regime is achieved faster than with antibodies ($k_{off} = 0$). This was confirmed by FRAP experiments (see below).

5. Measuring the Lifetime of Adhesive Bonds at Neuronal Contacts

5.1. Measurement of k_{off} by Bond Detachment Assays

The dissociation rate k_{off} of a given receptor–ligand interaction is the inverse of the bond lifetime (τ). Even in the absence of mechanical constraint, the molecules have a probability to unbind due to thermal fluctuations at the molecular interface, giving rise to an intrinsic lability of the bond that can be detected. If one can identify the initial time of bond formation, τ is simply the mean duration it takes for the bond to rupture. This is best measured at the single bond level *in vitro* using a laminar flow chamber at low shear rate, where microspheres kept in contact with the floor surface by single bonds suddenly flow away.[58] Using this assay, bond lifetimes have been found to be on the order of 1 s for typical adhesion molecules including cadherins,[58,93]and even shorter for selectins, which mediate the tethering and rolling of leukocytes on vascular surfaces during inflammation and immune surveillance.[94] However, some molecules such as cadherins can show a hierarchy of lifetimes and detachment forces, according to the molecular subdomains in contact.[95,96] Because the mechanical work done by the force could lower the energy barrier between bound and free states ("slip bond"), the parameter k_{off} was predicted to increase exponentially with the mechanical force placed on the bond.[63] This was validated experimentally for many molecules including selectins,[94,97] immunoglobulins,[98] and cadherins.[58] However, recently the existence of "catch bonds" was also demonstrated in P-selectin complexes with P-selectin glycoprotein ligand-1, in which force can prolong bond lifetime by deforming the molecules in such a way that they lock more tightly.[97] k_{off} also depends on the rate of force, albeit in a logarithmic manner.[57,99] These measurements were mostly obtained in artificial systems with purified proteins.

In cells, the simplest semiquantitative way to assay the dissociation of adhesive interactions is to perform rapid live surface labeling with adhesion ligands and then measure the time it takes for ligands to detach. Starting with a given population of ligands bound to cell surface receptors at time zero, the number of ligands still bound at time t is quantified and k_{off} is estimated by fitting the detachment curve by an exponentially decreasing function. In our hands, for similar ligand concentrations, neurons stain weakly for N-cadherin, a little more for TAG-1 and neurexin, and better with SynCAM,[100] reflecting differences in ligand–receptor bond lifetime. Labeling of fibroblasts with fibronectin monomers allowed the estimation of bond lifetime on the order of a few seconds.[42] Labeling was much stronger with fibronectin oligomers, which recognize integrin clusters, probably because avidity increases the lifetime of the overall molecular assembly.[42] By analogy, the *cis*-dimerization of many neuronal adhesion receptors including cadherins,[101] IgCAMs,[102] and neuroligins[83] is likely to contribute by cooperative effects to lower k_{off}.

A more quantitative approach to quantify bond lifetime is to image single fluorescent ligands interacting with the dorsal surface of a cell. The stepwise disappearance of the fluorescent signal indicates that the molecule has detached, and the statistics of these events gives the bond lifetime, i.e. of about 1 s for cadherin molecules,[103] in agreement with the flow chamber measurements. However, these observations are difficult to distinguish from photobleaching of single molecules, which also occurs as a single step (Figure 3C). An alternative is to use fluorescent nanocrystals (quantum dots), which are extremely photorobust, to label individual receptors. Using this approach, we observed the occasional detachment from the cell surface of quantum dots conjugated to adhesion proteins such as synCAM (Figure 5). These events can be attributed to the rupture of ligand–receptor bonds since the coupling of the adhesive ligand to the quantum dot via an antibody−Fc link should be quite stable. Another difficulty could stem from the fact that QD can blink repeatedly, corresponding to signal extinction that could be taken as a rupture event. However, fast acquisition rates show that QD diffusing away in the extracellular medium after adhesion rupture can be unequivocally distinguished from a blinking behavior (Figure 5). By computing the frequency of the breaking events, normalized by the number of bound quantum dots (N), one can calculate $k_{off} = 1/N(\Delta N/\Delta t)$. In the case of SynCAM homophilic adhesion, k_{off} is on the

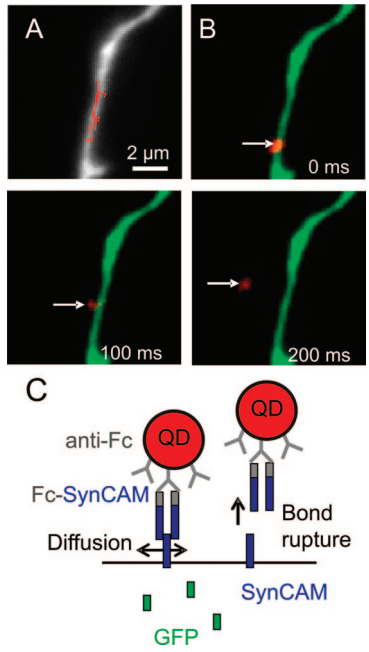

Figure 5. Example of individual bond dissociation between adhesion molecules. Primary neurons were transfected with synCAM1, a homophilic binding trans-synaptic protein, together with GFP to monitor the expressing cells. At 7 DIV, neurons were incubated with a soluble synCAM-Fc recombinant protein, followed by quantum dots conjugated to anti-Fc antibodies. The QD bound specifically to the transfected cell, revealing homophilic synCAM adhesion, and diffused laterally on the cell surface. (A) Neurite region showing the 30 s trajectory of a quantum dot (red) superimposed to the GFP signal (white). (B) Occasionally, we observed the detachment of QD from the cell surface, which could be clearly identified by QD diffusing away in the extracellular medium on the subsequent images (arrows). This was interpreted as the sudden rupture of SynCAM homophilic adhesion, since the anti-Fc bond is likely to be much more stable, and indeed QD detachment is rarely observed with QD bound to receptors via antibodies. (C) Sketch of the experiment.

order of 0.1 min^{-1}, a lower value than that of individual cadherin−cadherin[58,93] or selectin−carbohydrate interactions, indicating that synCAM provides long-lasting adhesion in agreement with its role of maintaining together pre- and postsynaptic compartments.[104]

5.2. Use of Photobleaching and Photoactivation

Bulk measurements of equilibrium turnover rates of adhesion proteins can also be extracted from a well-established technique called fluorescence recovery after photobleaching (FRAP).[105] Photobleaching consists in the irreversible extinction of a fluorophore upon continuous light excitation, which is due to a chemical oxidation reaction that takes places in the fluorophore group, and occurs as a statistical event after many cycles of absorption and emission of photons. The more intense the excitation light, the faster photobleaching will be. This property is used for FRAP, which consists in using a focused laser beam at high power to photobleach quickly and locally fluorescently tagged proteins.[30] Mobile proteins can exchange with their unbleached counterparts, leading to the recovery of fluorescence in the photobleached area at rates proportional to protein mobility.[106,107] Despite displaying complex photophysics, fluorescent proteins such as GFP are well suited for FRAP experiments, because they photobleach quickly with minimal oxidative byproduct, and their dark states are short enough and randomly distributed so that they are averaged out in the duration of a typical recovery. Mathematical modeling based on diffusion equations has been worked out to extract relevant parameters such as diffusion coefficient, anomalous diffusion parameters, and reaction rates from typical FRAP curves.[105,108,109]

In order to measure the lifetime of adhesive bonds, the general principle is to photobleach at a given neuronal contact a large population of GFP-tagged adhesion receptors undergoing continuous on/off interactions with specific ligands. Microspheres coated with purified recombinant adhesion proteins represent a biomimetic system of particular interest, as it allows a precise control of the type and density of ligand molecules presented to the cell and of the timing and duration of the interaction. This precision is not achievable at natural contacts that form at arbitrary moments and where different types of adhesion proteins can coexist in unknown stoichiometries. After initial bead−cell contact and the progressive recruitment of adhesion proteins as described in the previous paragraph, the contacts reach a dynamic equilibrium. This steady state is characterized by a bond density C_∞ and a continuous exchange between free and bound receptors at a rate $k_{off}[C_\infty]$, obtained by setting $d[C]/dt = 0$ in eq 3. In FRAP experiments, both bound and free receptors are photobleached at a bead contact at time zero. Assuming that diffusion occurs faster than the adhesive reaction, fluorescence recovery should occur in two separate steps: (i) a rapid phase due to diffusion of unbound adhesion receptors and fitted as a one-dimensional diffusive process[110] and (ii) a slower phase due to the replacement of bound receptors by unbleached receptors. This regime was modeled by a reaction term, assuming that the rate at which bleached receptors can leave the contact is proportional to the density of bleached receptors at time t.[111] The recovered intensity due to ligand–receptor exchange is then

$$([C_\infty] - [R]_t)\,[1 - \exp(-k_{off}t)] \qquad (5)$$

This model nicely fits the data for N-cadherin and L1 homophilic interactions and allows extracting the respective k_{off} values (Figure 6). The diffusion coefficient of unbound receptors can be obtained as a second parameter, but it is more variable and less informative. Control experiments with antibody-coated beads yield much reduced turnover rates, in agreement with the stability of antigen–antibody bonds. From a biological perspective, this approach demonstrated that the turnover rate of N-cadherin homophilic adhesion is regulated by interactions with the actin cytoskeleton via catenin partners,[111] and those of L1 are controlled by association with the clathrin endocytic pathway.[89] Overall, the lifetimes of adhesion receptors in neuronal contacts involving many molecules, on the order of several minutes to hours, are much lower than those found at the individual molecule level. This is also the case for integrins trapped in focal contacts,[112,113] suggesting that adhesion receptors in native clusters are stabilized by mechanisms other than the ligand–receptor transmembrane adhesion *per se*, e.g., *cis*-interactions with themselves or other membrane proteins, as well as coupling to cytoskeletal partners.

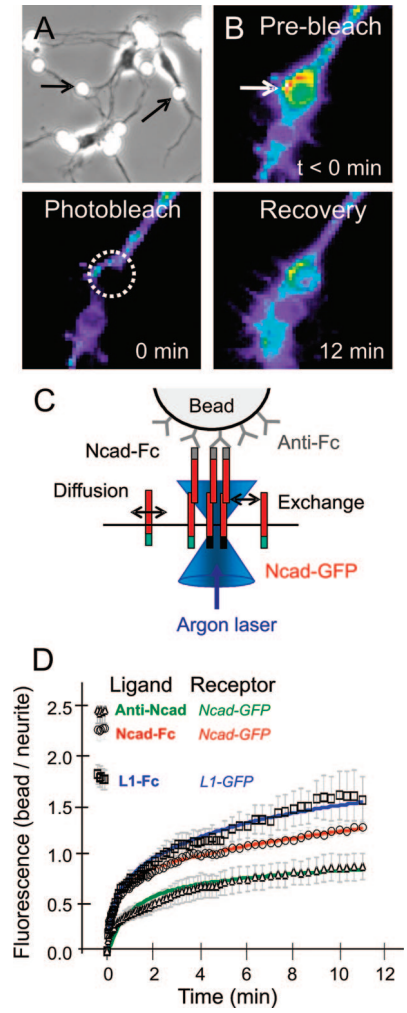

Figure 6. Measuring the turnover rate of adhesive interactions using fluorescence recovery after photobleaching. (A) 4 μm microspheres coated with N-cadherin-Fc (arrows) binding to rat hippocampal neurons. (B) N-cadherin-GFP receptors accumulate specifically around those microspheres (arrows). At time zero the GFP signal is photobleached with an argon laser focused at a high numerical aperture objective, and fluorescence recovery is followed for several minutes. (C) Schematic diagram of the molecular interactions and diffusion/reaction processes at the bead contact. (D) The N-cadherin-GFP or L1-GFP fluorescence signal is normalized by that on a control neurite region without bead. The rapid recovery (2 min) corresponds to the diffusion of free receptors, and the long-term regime to the slower turnover of molecular bonds. L1−L1 bonds recycle faster than N-cadherin homophilic adhesions, the latter being more labile than bonds formed by antibodies against N-cadherin.

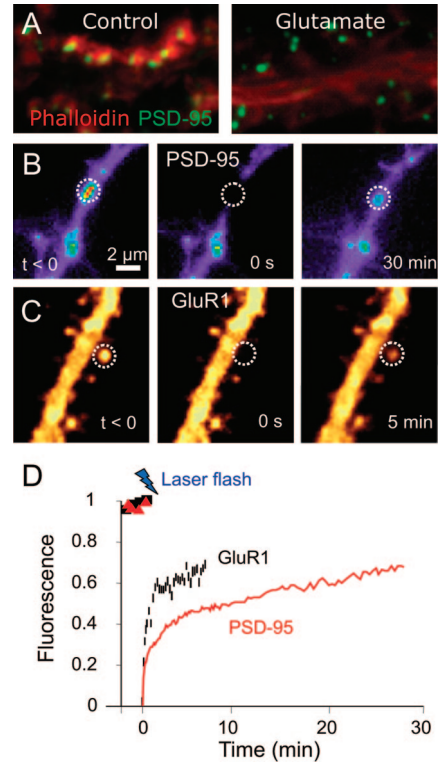

Figure 7. Different dynamics of postsynaptic molecules by imaging and photobleaching. (A) Glutamate treatment dissociates F-actin (red) from synapses but leaves PSD-95 clusters intact (green). Examples of FRAP at dendritic spines on PSD-95-GFP (B) and GluR1-pHluorin (C). (D) Corresponding recovery curves.

6. Measuring the Turnover Rates of Molecular Components in Postsynapses by FRAP

6.1. General Considerations

The postsynapse consists of a dense meshwork of cytoskeleton (notably actin) and scaffolding proteins (e.g., PSD-95, Shank, Homer, PICK/GRIP) that stabilize the different subtypes of glutamate receptors at the plasma membrane, mainly AMPA, NMDA, and kainate receptors, which are tetrameric ligand-activated ion channels involved in synaptic transmission.[114] FRAP can be used to investigate the mobility of such proteins at synapses. However, the overexpression of GFP-tagged molecules, essential to this fluorescence-based approach, may affect the intrinsic pool sizes and stoichiometries of binding partners. There is no ideal solution to this problem, but as discussed above, overexpression artifacts can be reduced by careful choice of the transfection method and the use of low-expression vectors that carry the gene of interest under the control of a weak promoter.[34] Furthermore, because most proteins in synapses are likely involved in multiple interactions, leading to complex binding states, it is often not possible to unambiguously isolate the rate constants of specific protein/protein interactions from a FRAP experiment. The fluorescence recovery curve may contain a mixture of different cryptic components that cannot be distinguished if their characteristic time scales are not well separated. Other issues are that multiple similar sites can bind to the same partner with different affinities (e.g., PDZ domains 1 and 2 of PSD-95 can both interact with stargazin), and there may be binding competition for the same site (e.g., NMDA receptors and stargazin for PDZ domains 1–2 of PSD-95).[115,116] To qualitatively compare different conditions and molecules, one usually extracts simply a fraction of mobile molecules and a characteristic turnover rate or half-life (Figure 7). We listed in Table 1 the average half-life of the major components of synapses, ranging from the most dynamic (monomeric actin and tubulin) to the most immobile (PSD-95 and NMDA receptors) that were recently measured by FRAP and compared them to values for Brownian motion of GFP in the cytosol and plasma membrane. In these measurements, it is often difficult to distinguish what is the respective contribution of binding/unbinding events, versus trafficking and delivery through endocytosis and exocytosis. This problem can be circumvented by tagging the extracellular domain of transmembrane proteins such as membrane adhesion proteins and glutamate receptors with a pH-sensitive GFP (pHluorin) whose fluorescence is quenched at the acid-

Table 1. Turnover Rates of Various Postsynaptic Proteins at Synapses

molecule	soluble GFP	membrane GFP	actin	tubulin	CaMKII	GluR1/2, Stargazin	H1c/ Shank	GKAP	PSD-95	NR1
half-life (min)	0.003	0.03	0.5	0.5	2	5–10	5–10	20	>60	>60
activity dependence	+	+	+	−	+	+	+/−	+/−	−	−
reference	118	119	131	218	134	139, 168	138	138	138	134

ic pH of endocytic compartments.[27] Then, only receptors exposed to the neutral extracellular pH are detectable in fluorescence microscopy.[117] Also note that FRAP experiments on diffusible molecules such as soluble GFP and membrane GFP have shown that the neck of the dendritic spines and their overall structure can restrict the flow of molecules from the neurite shaft to the head of the spine,[118,119] thus adding a further anomalous diffusion term in the already complex fluorescence recovery curve of postsynaptic components.[120] Still, despite these limitations, FRAP remains an essential method to probe the mobility of intracellular proteins, which are not accessible to labeling with external probes (see next paragraph). Remarkably, the turnover rates obtained optically by FRAP correlate fairly well with measurements of "functional recovery after inactivation", a physiological analogue of FRAP. These types of experiments are based on measuring the electrophysiological response elicited after local and specific inactivation of neurotransmitter receptors at synapses, using activity-dependent irreversible blockers of receptors, e.g., the photoactivatable compound ANQX for AMPARs,[121] MK-801 for NMDARs,[122] and MTSES for GABA receptors.[123]

A priori, the delivery and retrieval of the various molecular components at postsynapses could involve either passive diffusion or intracellular vesicular trafficking, through endocytosis and exocytosis.[124] Indeed, components of the trans-golgi network (TGN), an anabolic intracellular organelle where trans-membrane and secreted proteins are sorted and modified, have been detected at sites of axo-dendritic contacts.[125] Moreover, Golgi oupotsts are concentrated at dendritic branchpoints,[126] and endocytic pits are closely associated with synapses and regulate the availability of receptors.[127] However, FRAP and related experiments suggest that the replacement of functional receptors at synapses occurs mainly through surface diffusion, because the rates of receptor delivery by exocytosis, on time scales of hours, are intrinsically slower.[128–130] Exchange rates obtained for postsynaptic density proteins are usually not affected by inhibiting protein synthesis or proteasome-mediated protein degradation[10] and greatly exceed rates of replenishment from somatic sources, indicating that the dynamics of synaptic molecules may be dominated by local protein exchange and redistribution, whereas protein synthesis and degradation serve to maintain and regulate the sizes of local pools of these proteins.

6.2. Specific Examples

One way to gain insight into intrinsic protein–protein associations is to use selective biological tools to affect protein mobility and isolate the mechanisms and essential protein partners in this process. Several strategies can be followed.

(1) Electrophysiological stimulation of neurons to elicit postsynaptic activation. This can be done for example by elevating the potassium concentration to cause axonal depolarization or by electrical protocols (5–100 Hz wide field stimulations, photoconduction triggered on silicon substrates) or chemical treatments (a mixture of bicuculline to block GABAergic inhibitory synapses together with glycine or NMDA to favor glutamatergic transmission). Such treatments, in particular by inducing calcium entry through NMDA receptors and voltage-gated ion channels, have broad impacts. For example, neuronal activation triggers changes in synapse shape and size, accompanied by a stabilization of actin[131–133] and CaMKII[134] at dendritic spines, the recruitment and immobilization of β-catenin,[135] and the endocytosis of N-cadherin.[136] One intriguing aspect here is that the actin cytoskeleton turns over quite rapidly at synapses, which renders all existing protein–protein interactions that anchor and stabilize other postsynaptic proteins subject to constant recycling. For example, the catenin−cadherin complex in adhesion zones is linked to actin in a very dynamic fashion.[137]

(2) Use of selective pharmacological compounds to inhibit a specific pathway, e.g., ionotropic receptor channels, exo/endocytosis, cytoskeleton. For example, the use of latrunculin to depolymerize the F-actin cytoskeleton was shown to eliminate the dynamic fraction of GKAP, Shank, and Homer 1c but not PSD-95,[138] suggesting that actin anchors a mobile pool of PSD molecules at synapses (Figure 7A).

(3) Overexpression of dominant negative proteins, siRNA, or use of knockout mice to interfere with the kinetics of a protein or to completely remove one specific protein. For example, in neurons from mice lacking gelsolin, a protein known to sever actin and cap its barbed end in a calcium-dependent manner, activity dependent stabilization of actin was impaired.[131]

The use of a photoactivatable isoform of GFP (PA-GFP) that is only detectable after irradiation with UV light (405 nm) or infrared light (750 nm) through two-photon excitation can be used to visualize the dynamics of specific pools of proteins of interest.[32] The decay in fluorescence intensity after photoactivation is the mirror image of a FRAP curve and gives similar information, with the advantage that one can follow the redistribution of the photoactivated molecules. This is not possible in FRAP, where the photobleached molecules dissolve in a uniformly bright background. We used PA-GFP fused to N-cadherin to estimate the k_{off} of N-cadherin homophilic bonds at neuronal contacts.[111] Photoactivation was also used to measure the turnover rates of Synapsin I and ProSAP2/Shank3, prominent presynaptic and postsynaptic matrix molecules, respectively.[10] These experiments revealed that both molecules are continuously lost from, redistributed among, and reincorporated into synaptic structures at time scales of minutes to hours. Similarly, fluorescence loss in photobleaching (FLIP), which consists in repeatedly photobleaching the same area while measuring fluorescence decrease in adjacent areas, when performed on Glur2-pHluorin demonstrated exchange of AMPA receptors between nearby synapses.[139] Finally, photoactivation of GluR2 labeled with PA-GFP at the *Drosophila* larvae neuromuscular junction (NMJ) showed that GluR2-containing AMPARs slowly enter growing postsynaptic densities mainly from diffuse extrasynaptic pools.[140] The recovery rates measured for GluRs in these large glutamatergic

synapses as well for acetylcholine receptors in vertebrate cholinergic NMJs[141] are much lower than in synapses from primary CNS neurons,[140,142] possibly due to a size effect limiting the exchange of receptors, or more likely to intrinsic structural and functional differences. Indeed, these synapses, which require very robust and reliable synaptic transmission, show very little plasticity and display basal turnover rates that are intrinsically very slow.

7. Measuring Transient Interactions of Neurotransmitter Receptors to Postsynaptic Scaffolds by Single-Molecule and Single-Particle Tracking

7.1. Methodological Issues

An alternative to ensemble approaches such as FRAP or photoactivation relies on the tracking of individual molecules. This methodology consists in attaching a small particle specifically to a molecule of interest and following the movement of this probe on the neuronal surface. Attachment of the probe can be achieved by means of (1) antibodies against external epitopes of endogenous molecules or tags (HA, myc, 6-His, GFP, RFP, etc.) fused to the protein of interest, (2) small ligands to specific receptors (α-bungarotoxin, which naturally binds to acetylcholine receptors, can recognize a 7 kD binding site fused to the N-terminus of a glutamate receptor),[143] (3) avidin–biotin linkage, after biotinylation using biotin ligase of the target protein containing a 15-amino acid acceptor peptide (AP) sequence,[144,145] or (4) adhesion proteins with long-lasting ligand–receptor interactions, e.g., SynCAM or neurexin, such as described above. Thus, one major advantage of this technique with respect to all other methods that require overexpression of fluorescently tagged proteins is that it allows measurement of the mobility of endogenous molecules. Historically, 0.2–0.5 μm latex beads were used and could be placed on the cell surface by optical tweezers and detected by video-enhanced differential interference contrast (DIC) microscopy.[146] The relatively large size of these particles however prevented their access to restricted cellular compartments, such as adhesive junctions or the synaptic cleft. Colloidal gold particles of 40 nm have also been used but are still too large and can form higher order aggregates. Another issue related to their size is that these probes can cross-link several receptors because of their multivalency. Hence, smaller probes and smaller ligands were needed. A first approach consisted in the use of antibodies or ligands conjugated to single organic fluorophores (e.g., cyanine 5) bound to only one or two receptors.[147,148] Such ligands are small enough such that they should access synaptic compartments.[149] Moreover, this strategy provides the advantage to allow tracking molecules with a position accuracy only limited by the signal-to-noise ratio at which the molecules are detected, in practice below 40 nm in live cells for cyanine dyes using 30 ms integration times (Figure 8A). This allows endogenous receptor trajectories to be measured inside synapses, whose diameters are on the order of 300 nm.

In order to assess that single molecule are detected, it is important to thoroughly characterize the signal arising from an individual molecule. The signal should display a diffraction-limited spot and show digital photobleaching; that is, it must be constant over time, then drop instantaneously to background levels. All molecules should have comparable

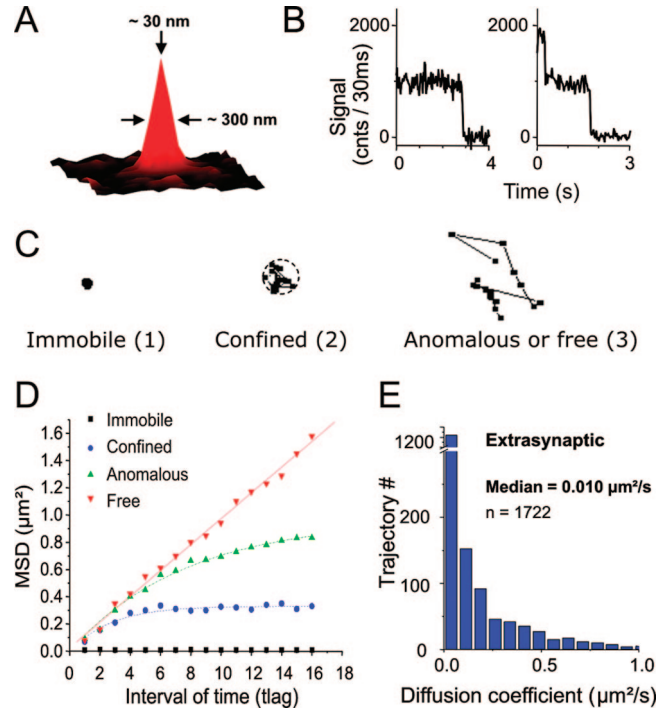

Figure 8. Single-molecule detection and heterogeneity in protein mobility revealed by single-molecule tracking. Endogenous glutamate receptors in 10 DIV primary neurons were labeled with antibodies to their N-terminal domain, conjugated to a single Cy5 fluorophore. (A) 3D plot of the fluorescent signal obtained from such a single Cy5 in 30 ms. (B) Fluorescence intensity plot over time, showing that a single cy5 molecule has a well-defined signal and photobleaches in a single step (left). (Right) Two Cy5 detected unambiguously in the same spot show initially twice the signal of a single Cy5 and photobleach sequentially. (C) Representative examples of the different types of trajectories obtained (time windows of 2 s). (D) Corresponding mean-squared displacement over time for the typical trajectories shown in (C). (E) The diffusion coefficient computed from the initial slope of the MSD versus time plot is plotted as a histogram, reflecting enormous heterogeneity at the individual level and allowing comparison between biological conditions.

fluorescence levels such that two molecules present in the diffraction-limited spot should display dual photobleaching steps of equal amplitudes (Figure 8B). One major drawback is that the fluorescence signal linked to only one fluorophore photobleaches quickly, giving rise to trajectories that are at most a few seconds (although new organic dyes may show improved lifetime). This is too short to explore the complete kinetics of receptor entry in, and exit of, synapses.

The most recent technical development involves the use of semiconductor fluorescent nanocrystals known as "quantum dots", which can be used for *in vivo* applications.[150,151] These are resistant to photobleaching and can be observed for several minutes, with typical sampling frequency of 30–100 Hz depending on the field area. Quantum dots have a broad excitation spectrum but a tight emission spectrum that depends on the particle core size, allowing multicolor imaging, and are commercially available with various coating properties (avidin, secondary antibody F_{ab} fragment to most species). Given the several layers (inorganic, organic, and biological ligands) added to these particles to render them water-soluble and functional, they reach relatively large sizes, i.e., approximately 20 nm, which is the limit to enter cell junctions. They were shown to penetrate inhibitory synapses[152] and to have restricted accessibility at excitatory synapses.[149,153] One concern with quantum dots is that they

blink at random times and for arbitrary durations: while the observation of blinking is proof of monodispersion of the particles, this can make tracking difficult and induce potential artifacts in trajectory reconstruction if not done properly.[149] Although we observed quantum dots inside cells, the mechanisms by which they penetrate is not well understood and may involve endocytosis. By controlling the selective delivery of quantum dots conjugated to specific intracellular proteins (e.g., molecular motors, scaffold proteins, neurotransmitter receptors), one would be able to follow the whole cycle of a single molecule and possibly resolve the interplay between trafficking events (endo/exocytosis) and surface diffusion, which is still unclear with regard to glutamate receptors.

It is thus clear that novel strategies are still needed to efficiently track individual molecules. To reach this goal, ultrasensitive photothermal imaging methods were developed to detect nanometer-size gold particles with an optical microscope.[154–156] The most sensitive one, referred to as light-induced scattering around a nanoabsorber (LISNA), was used to ultimately detect gold nanoparticles as small as 1.4 nm diameter in polymers.[156] LISNA is based on a two-color confocal microscope since it uses a combination of a focused time-modulated excitation beam that heats the absorbing gold nanoparticles and a focused nonresonant probe beam. The heating induces a time-modulated variation of the refraction index around the absorbing nanoparticle. The interaction of the probe beam with this index profile produces a scattered field with sidebands at the modulation frequency. The scattered field is then detected in the forward direction through its beat note with the transmitted probe field, which plays the role of a local oscillator akin to a heterodyne technique. Raster scan of a sample containing nanoabsorbers produces 2D LISNA images of the sample (Figure 9). The signal is proportional to the volume of the particle and not subject to photobleaching. This technique has allowed scanning of fixed and live samples with confocal resolution, as well as tracking of individual 5 nm gold nanoparticles fused to antibodies directed against AMPA receptors at the surface of live neurons, at video rate during arbitrary long recording times.[157] Another advantage is that the chemistry for conjugation of gold particles to biological ligands has been well worked out, so that tracking a 5 nm gold particle attached to a 5 nm ligand (e.g., antibody F_{ab} fragments) within a single synapse becomes possible. Furthermore, because of the straight relationship between the photothermal signal and the particle number, one can in principle achieve a precise estimation of the numbers of receptors at synapses using this technique. To reach this goal, one has to precisely control the binding stoichiometry of antibodies or ligands to the nanoparticles, then to use a dense labeling of cell surface receptors under saturating conditions, so as not to miss any free receptor. A last point is that the use of gold may allow retrospective cryoelectron microscopy to be performed on the same samples, in order to obtain a nanometer resolution map to correlate with live images.

7.2. Trajectory Analysis and Biological Behavior

The immediate output of single-particle tracking experiments is a reconstructed two-dimensional trajectory of the probe over time. An important parameter in the theory of diffusion is the mean-squared displacement (MSD = $\langle x^2 + y^2 \rangle$), which describes the area explored by the particle per unit of time. For an experimental trajectory identified by

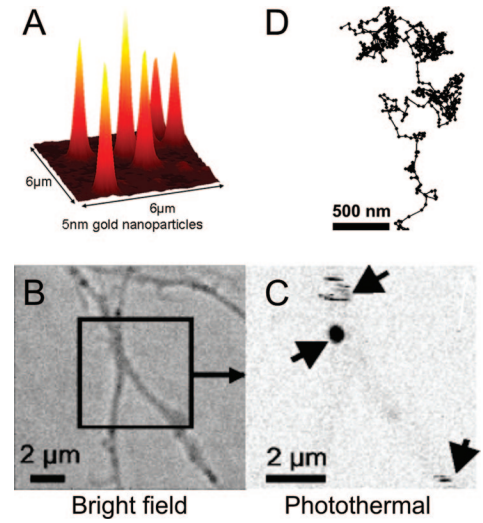

Figure 9. Photothermal imaging of single gold nanoparticles on cell surfaces. (A) Photothermal image of 5 nm gold particles immobilized in polymer. (B,C) Primary neurons incubated with gold nanoparticles coated with antibodies to the GluR2 subunit of AMPA receptors. (B) Bright field image of a neurite region. (C) The corresponding photothermal image obtained by scanning the field during 10 s. The well-defined particle in the center is immobile, while the two other particles showing horizontal streaks are mobile (arrows). (D) Example of a 300 s trajectory for a single 5 nm particle on the surface of a neurite. By analogy with a GPS, tracking is achieved by repeating three rapid readings (5 ms each) of the photothermal signal around the nanoparticle, followed by calculation of actual position, then by repositioning the piezo-driven stage to the new position, and so on.

coordinates (x_i, y_i) at time $t = i\Delta t$, where Δt is the time interval between two successive acquisitions and $i = 1$ to n is the number of steps, this expression becomes

$$\mathrm{MSD}(i\Delta t) = \sum_k [(x_{k+i} - x_k)^2 + (y_{k+i} - y_k)^2)]/(n - i) \quad (6)$$

For pure Brownian motion, the mean-squared displacement is linear over time and the slope gives the translational diffusion coefficient D (in $\mu m^2/s$). However, since the plasma membrane is not a homogeneous and continuous medium,[158–160] the movement of individual receptors often deviates from this model behavior and shows restricted or anomalous diffusion, which appears as an inflection of the MSD curve for large time intervals.[161] High-speed acquisition can reveal very short immobilization events, on the 100 ms time scale, for example in lipid rafts or protein clusters.[162,163] Alternatively, if receptors couple to moving elements of the cytoskeleton (actin flow or microtubule motors), the directed motion in the trajectory contributes a parabolic component in the MSD curve.[164] In a first global approach, an instantaneous diffusion coefficient can be derived from the initial points of the MSD plot for each trajectory over a large number of particles, and different biological conditions can be compared by the histogram of the yielded diffusion coefficients (Figure 8C−E). One can also fit the MSD plot of individual trajectories to get detailed information about the mechanisms responsible for constrained diffusion, movement, or immobilization. In addition, the plot of instantaneous diffusion coefficient of a single particle over time can reveal complex behavior where receptors alternate between phases of free diffusion with high D (typically 0.01–0.1 $\mu m^2/s$) and transient immobilization with very low D (<0.001 $\mu m^2/s$).

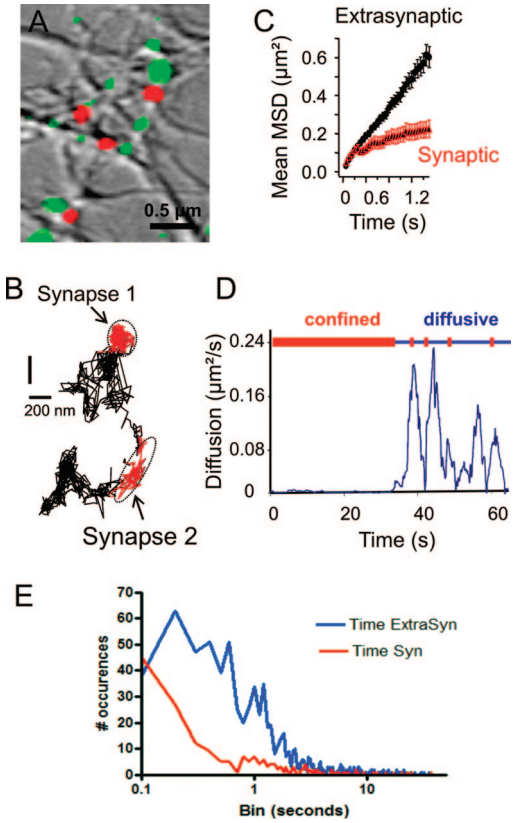

Figure 10. Details of receptor movement followed by single quantum dot tracking. (A) Superimposition of the quantum dot image (red) and synapse staining (green) to the DIC image showing the dendrite network in a 3-week-old primary neuron. (B) 2 min trajectory of a single quantum dot bound to the GluR1 subunit of AMPA receptors. Note that the particle stays confined at synaptic compartments (red) and moves freely in between (black trace). (C) This qualitative behavior is confirmed quantitatively by plotting the MSD versus time, for an average of many particles. The MSD is linear for extrasynaptic trajectories and saturates for synaptic stretches of trajectories, indicating confinement. (D) The instantaneous diffusion coefficient can be calculated over time along the trajectory and correlated with the presence of a synapse or postsynaptic cluster. By setting a threshold diffusion coefficient, one can identify stretches of trajectories that are below the threshold, i.e., confined (red) or above the threshold, i.e., showing Brownian motion (blue). (E) Distribution of dwell times of QDs inside (red) and outside synapses.

This phenomenon can be further characterized by calculating a confinement index, a mathematical function that measures the degree of deviation from a purely Brownian behavior.[165] Such an index unambiguously identifies confinement periods of the neurotransmitter receptors.[166] The transitions between the confined and free states are quite fast, typically within two video frames, suggesting that they are mediated by rapid and specific binding between proteins, namely, interactions between neurotransmitter receptors and scaffold proteins located at specific sites beneath the neuronal membrane.

An important aspect of single-particle tracking is that, because it is mostly an imaging-based technology, data extracted from the trajectories, i.e., the confinement periods of each trajectory, bear spatial information and can be related to specific cellular features acquired in another spectral channel. Typically, one can superimpose the trajectory of a quantum dot to a DIC image of the neurite network or to the image of synapses stained with a specific marker (Mitotracker, FM dyes, or postsynaptic proteins fused with fluorescent proteins) (Figure 10). Using such correlation

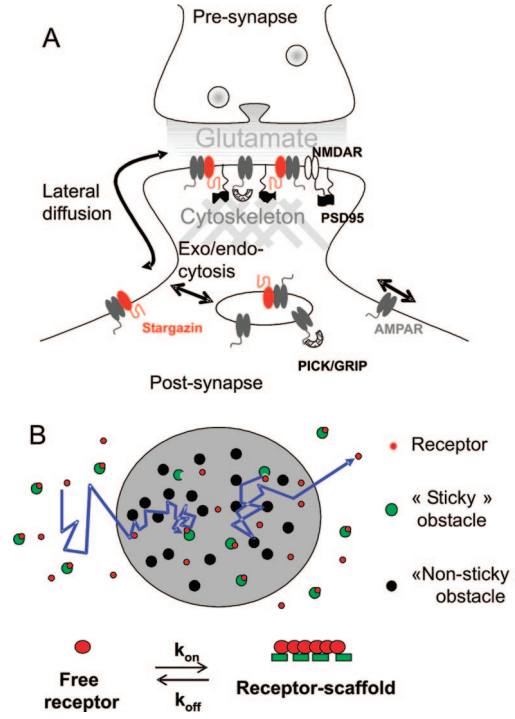

Figure 11. Summary sketch of neurotransmitter receptor behavior in the neuronal membrane. (A) Side view of a synapse. The main interacting partners of AMPA receptors and pathways controlling AMPAR mobility (surface diffusion versus endo/exocytosis) are shown: stargazin is the auxiliary subunit of AMPA receptors, PICK/GRIP are involved in delivery of AMPAR to the cell surface. Both stargazin and NMDA receptors can bind the essential scaffold protein PSD-95. (B) Top view of a postsynaptic density (gray circle), rich in scaffold proteins (red circles), and allowing the transient trapping of glutamate receptors (red circles). The black circles represent other membrane pickets such as adhesion proteins, to which the receptors cannot anchor to, but onto which they bounce. This effect on the trajectory contributes to anomalous diffusion.

maps, it was found that the stabilization of glycine receptors occurs specifically in areas with strong gephyrin-GFP fluorescence,[166] mGluR5 receptors stop on Homer clusters,[167] and GluR2-containing AMPA receptors visit synapses in confined movements.[146,147]

Essentially the same methods as described above for FRAP can be used to selectively isolate the contribution of given elements in a specific interaction. For example, using mutants of PSD-95 and stargazin, the auxiliary subunit of AMPA receptors, we showed recently that AMPARs are transiently immobilized at synapses through a specific interaction between stargazin and PSD-95[168] (Figure 11A). On the basis of these data, we have come up with a model where neurotransmitter receptors undergo continuous exchange between Brownian diffusion in the extrasynaptic membrane and transient trapping by scaffold proteins at synaptic sites (Figure 11B). The motion inside synapses is anomalous due to the presence of many obstacles in such a crowded environment.

7.3. Trajectory Modeling and Determination of Reaction Rates

Once the biological system has been sufficiently resolved so that one can confidently attribute the stabilization periods of a trajectory to specific protein/protein interactions, the in/out transitions between compartments contain information about the rates of attachment and detachment of these two

proteins. This information lies in the distribution of diffusive and confined dwell times (Figure 10E). As in laminar flow experiments, if the receptor binds to a single scaffold protein at time zero when it enters a cluster, the distribution of individual arrest durations should be fitted by a single exponential, $\exp(-k_{off}t)$. If the fit is more complex, as is often the case, it means that multiple bonds or multiple binding states are involved. On the other hand, the distribution of diffusive periods contains information about diffusion properties as well as binding *per se*, as described for ensemble measurements (see section 4). It is theoretically possible to separate the two aspects by using models of diffusion/trapping and fitting the distribution of dwell times with simulated data to get the intrinsic k_{on} value. We simulated trajectories, where receptor movement is modeled as a two-dimensional random walk, with the possibility to bind to periodically spaced quasi-immobile scaffolding elements and detach from them (Figure 12A). This model yields the cumulative distribution of diffusive periods, as well as the overall fraction of time spent in the confined state (Figure 12B). When the intercluster distance decreases, e.g., corresponding to an increase in synapse density in the course of aging of neuronal cultures, this parameter increases (Figure 12C) as observed experimentally for GluR2-containing AMPA receptors.[146] One can refine the model by adding extra parameters if the chemical system is more complex, e.g., in the case of the interaction between glycine receptors and gephyrin, which shows multiple binding states.[169]

8. Measurements of Diffusion and Reaction Rates by FCS and FCCS

8.1. Principle and Methodological Requirements

Standing as an intermediate between ensemble and single-molecule approaches, fluorescence correlation spectroscopy (FCS) takes advantage of the fluorescence intensity fluctuations that occur within a small detection volume, i.e., the change in number of detected photons when fluorophores enter and leave the detection volume[170,171] (Figure 13A,C). The autocorrelation of these fluctuations yields the average dwell time of a fluorescent molecule in the detection volume and thereby the diffusion constant.[172,173] Hence the control of the excitation volume is critical to this method. In general, laser light is focused through a microscope objective to excite fluorescence in a diffraction-limited spot, and a pinhole in confocal configuration rejects fluorescence from regions above and below the focal plane, so as to define a confocal volume of about 0.5 μm width and 1 μm height, i.e., around 0.2 femtoliters. The width of the spot can be varied by controlling the amount of back-filling of the laser into the objective. A nonlinear dependence of the yielded diffusion coefficients on the spot size demonstrates inhomogeneity of the medium, as shown for the plasma membrane.[174,175]

FCS can also be used with two-photon illumination, an advanced microscopy technology where the simultaneous absorption of two photons generated by femtosecond laser pulses provides the energy to excite a fluorophore. In this special case, the emission volume is intrinsically smaller and in fact identical to the excitation volume because the probability for a fluorophore to absorb two photons quasi-simultaneously decays exponentially with distance from the focal spot (Figure 13B). A pinhole to reject out-of-focus light is thus not required, and even scattered emission light can be collected and detected. Two-photon microscopy is an important technological advance especially in the neurosciences since the excitation wavelength in the IR range is scattered less in biological material and can thus penetrate deeper into tissue of live animals or brain slices.[176] It also allows uncaging of bioactive compounds such as caged glutamate to probe the physiological properties of ion channels.[177–179] In both single-photon and two-photon FCS the light emitted by fluorophores when they reside in this volume is detected with sensitive photomultiplier tubes

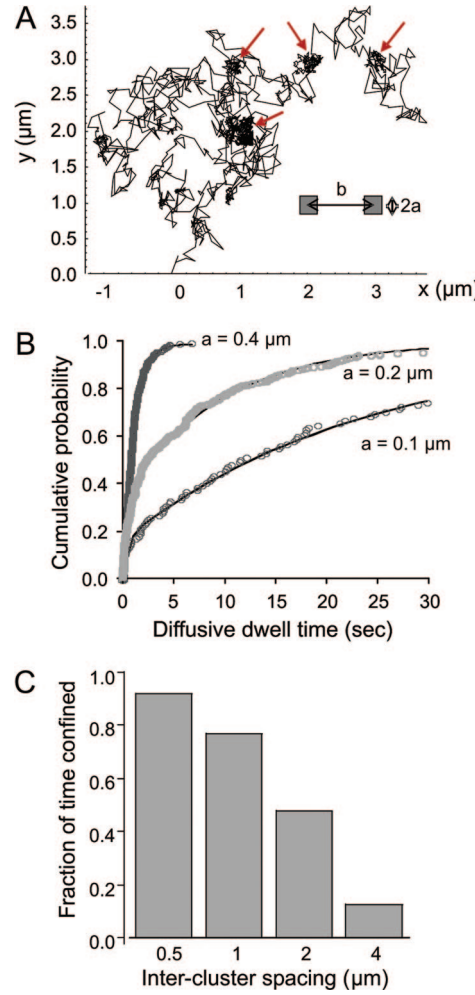

Figure 12. Simulation of single-receptor membrane diffusion and trapping by scaffolding clusters. A computer algorithm based on previous work[219] was written within the Mathematica software. The total time of a trajectory (typically 100 s) is divided into time steps of $\Delta t = 30$ ms, corresponding to the experimental acquisition rate. On a 2D grid, areas of possible anchoring of square geometry (side $= a$ μm) and regularly spaced (one area every b μm in both x and y) are defined. These areas represent the clusters rich in scaffold proteins observed experimentally. When it is outside of these specific areas, the receptor follows a random walk with average diffusion coefficient $D = 0.02$ $\mu m^2/s$. When the receptor reaches one cluster, it is allowed to bind with rate constant k_{on}. During binding, the receptor is set to diffuse with a 10 times lower coefficient than that of the cluster itself. The receptor stays confined in the area until the probability for detachment ($k_{off}\Delta t$) exceeds a random number generated from a uniform distribution. The receptor then undergoes another random walk until it binds again, and so on. (A) Example of simulated trajectory. Note the longer residency of the receptors in the cluster areas (arrows). (B) Cumulative distribution of simulated diffusive dwell times as a function of the cluster size. Plain curves represent biexponential fits. (C) Calculation of the fraction of time spent by a receptor in the confined state, along its whole trajectory, as a function of intercluster distance b.

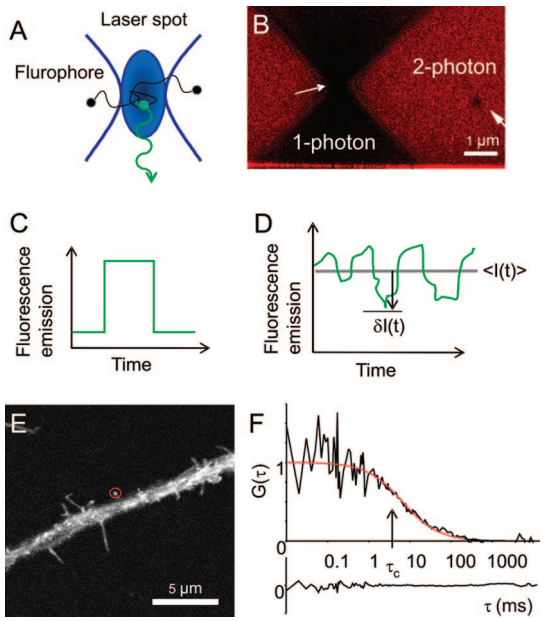

Figure 13. Principle of FCS and FCCS. (A) Schematic diagram of a fluorophore crossing a confocal excitation volume. It can emit photons (green arrow) only when it resides in this volume (C). (B) Laser spots in monophoton and biphoton illumination, obtained with an SP2 confocal laser-scanning microscope with the 488 nm line of an argon laser (left) or a Coherent Mira 900 titane-sapphire laser tuned at a 900 nm in biphoton excitation (right). The sample is a goat anti-mouse antibody conjugated to Alexa 488 trapped in a 15% polyacrylamide gel, resulting in irreversible photobleaching of the illuminated areas. (E) Example of an FCS measurement of GPI-GFP diffusion within a synaptic spine (red circle) performed on a Leica SP2 confocal laser-scanning microscope with a Leica FCS module. The neuron is 3 weeks *in vitro*. (F) An autocorrelation curve $G(\tau)$ of a single 10 s measurement at the spot shown in (E). The curve was fitted with a one-component model for two-dimensional diffusion, which yields a D of 1.1 $\mu m^2/s$. The residuals of the fit are shown below.

(PMT) or avalanche photodiodes (APD) to reach single-photon counting with time resolution ≥ 1 MHz. The decisive feature of FCS is that not the average fluorescence intensity $\langle I(t)\rangle$ but rather the intensity fluctuations around this mean $\delta I(t)$ constitute the signal (Figure 13D). The larger these fluctuations, the more precise the measurements will be. Hence, very dilute samples are desirable, with typically 1–10 molecules in the confocal volume (~1 fL), corresponding to concentrations in the nanomolar range. This constraint to work with scarce fluorophores becomes a challenge in biological samples, where the transfection of fluorescently tagged proteins has been optimized to yield high expression levels. One must choose cells emitting very low fluorescence intensity, but then one faces the problem that cells contain autofluorescent proteins (e.g., flavins) that can contaminate the specific signal. An alternative is to prebleach the sample before doing the FCS measurement, with the drawback of phototoxicity by the production of oxidative compounds. The best choice would be to decrease the excitation volume below the diffraction limit, which can be achieved for example using substrates containing regular arrays of holes of nanometer size.[180–182]

Another possibility is the reduction of the emission volume by stimulated emission depletion microscopy (STED), which consists in inducing stimulated emission around the excitation spot, using a second laser with a wavelength at the red end of the emission spectrum that immediately brings the fluorophore to its ground level.[183,184] With this technology, a resolution of down to 40 nm has been achieved[185] and the application to FCS has been reported.[186] A smaller detection volume then allows working with higher concentrations of fluorescent species and slower moving molecules, an important concern when working with transmembrane proteins that exhibit diffusion coefficients smaller than 0.1 $\mu m^2/s$. A different approach for the reduction of the detection volume is total internal reflection FCS (TIR-FCS), where the rapid decay of the evanescent field of a reflected laser beam at an interface reduces the z-dimension naturally to 100–200 nm.[187] This technique is powerful in the detection of surface binding,[188] but its use in cells is limited to the investigation of cell−substrate contacts.

8.2. The Autocorrelation Function

From the intensity fluctuations over time, two types of measurements can be computed. The first is an autocorrelation function (ACF), which is the convolution product of the intensity fluctuations $\delta I(t)$ by the same fluctuations displaced by a time length τ, $\delta I(t + \tau)$, and integrated over the duration of the experiment:

$$G(\tau) = \langle \delta I(t)\, \delta I(t + \tau)\rangle / \langle I(t)\rangle \qquad (7)$$

To understand the meaning of this expression, let us take the example of one molecule traveling through the excitation volume. If it enters at time zero and takes a characteristic time $\tau_c = a^2/D$ to exit the volume by Brownian motion (where a is the width of the confocal volume and the D the diffusion coefficient), then the fluorescence emission will be correlated with itself for times $\tau \leq \tau_c$ and no longer correlated for times $\tau \geq \tau_c$. This line of reasoning also applies for small numbers of molecules constantly entering and exiting the excitation volume at random times. Thus, the autocorrelation function has its maximum at time zero and drops to zero at infinite times, with a cutoff value τ_c, the characteristic diffusion time, which is inversely related to the translational diffusion coefficient of the molecular species in the sample (Figure 13E,F). Since the stochastics of molecule motion are measured, a key assumption is that the sample is homogeneous and continuous and the number of molecules within the emission volume negligibly small compared to the pool in the sample. The experimental curve is generally fitted by a model of 2D or 3D diffusion that includes the geometric profile of the illuminated area and several adjustable parameters including τ_c. Another important parameter comes from the value of the autocorrelation function at time zero, which is inversely related to the average number of molecules in the excitation volume $G(0) = 1/\langle N\rangle$. This property can be used to estimate the concentration of molecules in the sample or to indirectly estimate the confocal volume, depending on which one is known best. The diffusion time τ_c depends on the size and shape of the molecular species, with larger molecules exhibiting longer diffusion times, and this can in theory be used to estimate homo-oligomerization or binding to a much larger molecule, from an increase in τ_c. This has been applied to dynamics of oligonucleotides in the nucleus of live cells.[189]

There are two major difficulties associated with FCS that are linked to the photophysics of the fluorescent proteins: one is the existence of triplet and dark states, and the other is photobleaching. Both processes occur with characteristic time scales, which are likely to depend on the excitation

intensity. While the first will add autonomous and specific decay times to the autocorrelation function, and thereby contaminate the effects due to diffusion alone, the latter will lead to both an offset in the ACF and underestimation of τ_c. Corrections can be made by integrating these effects into the fitting algorithm, but they cannot always be isolated from the characteristic diffusion time. It is therefore essential to choose the most stable and photorobust fluorophores available and to carefully control the illumination intensity. In general it is advisable to use the lowest excitation light intensity that delivers a detectable signal and to start the autocorrelation immediately after switching the laser on. One problem inherent to biological samples is that the reservoir is limited and underlies structural constraints and that the diffusion of membrane molecules is comparatively slow; therefore prolonged measurements are necessary. This requires a very high photostability not met by most fluorescent proteins and may lead to noise from structural changes in the cell during the measurements, which may last up to 5 min. Also, it might be necessary to bleach an immobile pool of molecules before the mobile population can be accessed; this will be obvious from the photon count rate and the offset in the autocorrelation curve.

8.3. The Photon-Counting Histogram

Another function that can be computed from FCS experiments is the photon-counting histogram (PCH),[190] which numerically represents the probability of detecting one photon, two photons, k photons, etc., in the confocal volume, within a given time interval during the FCS measurement (usually the clock rate of the autocorrelation). It is again related to the average number of molecules $\langle N \rangle$ in the sample, but more importantly to the molecular brightness of the fluorescent species ϵ, which is defined as the average number of photons detected per unit of time and per molecule. In other words, the PCH is the convolution of the individual fluorescence-intensity peaks detected from fluorescent molecules passing through the detection volume during the measurement. Thus a monodispersed fluorescent monomeric molecular species such as GFP will yield a given PCH, which is characteristic of the photophysics of this molecule and that can be theoretically modeled.[191] If two species of different molecular brightness (such as dimers and monomers of the same molecule) are present in the sample, this can be detected by deconvolution of the PCH.[192] This approach could be applied in theory to count the number of postsynaptic scaffold molecules and determine their amount of cross-linking. For example, PSD-95 is known to self-assemble through its N-terminus sequence,[193] and Homer is known to dimerize.[167] The originality would be to perform repeated measurements on the same synapse, to get dynamic estimates of protein oligomerization, e.g., in response to specific neuronal stimulations.

8.4. Fluorescence Cross-Correlation Spectroscopy

Fluorescence cross correlation spectroscopy (FCCS) is a complementary approach that allows evaluating if several molecular components are associated when they move through the detection volume. The principle is the same as for FCS, but instead of calculating the autocorrelation function for one species, the intensity fluctuations from two molecular species labeled with different fluorophores are separately detected by two APDs and cross-correlated; that is, only if a photon is detected in both channels within an observation period is this counted as an event.[194] If the molecules travel together through the excitation volume, fluorescence bursts are detected in both channels and there should be a high initial value in the cross correlation curve, which can in combination with the autocorrelation data be used to estimate the fraction of molecules that are associated. To detect comigration, it is critical to excite the two fluorophores within the same volume. This can be achieved with two perfectly collinear laser beams and well-aligned and corrected optics. Alternatively, a single two-photon laser beam can be used to excite both fluorophores simultaneously with the advantage that fluorophores usually have broad two-photon absorption spectra, but then photobleaching can be non-negligible and the illumination intensity cannot always be optimized for each fluorophore. Recently, a variant of a corral fluorescent protein (Keima) with a very large Stokes shift (peak excitation 480 nm, peak emission 610 nm) has been designed, which allows the use of a single argon laser to excite both GFP and Keima in the same confocal volume and detection of two widely separated emission channels.[195] It has been successfully applied to the detection of the calcium-dependent specific interaction between calmodulin and calmodulin-dependent Kinase 1 in vitro,[195] a model system also used in a careful study of the complex stoichiometry of the system.[173] In live cells, the expression levels of the two fluorescently tagged proteins will have to be adjusted according to the respective molecular brightness to get similar photon counts in the two channels while not neglecting the expected stoichiometry of interaction. At the same time, the laser power has to be chosen such that it photobleaches neither fluorophore, which may not always be possible since most fluorophores have complex two-photon absorption spectra. Although still in its early days, FCCS seems a very promising technology for the quantification of protein–protein interactions in live cells in general and specifically at cell−cell contacts such as synapses. A long series of *in vitro* studies have demonstrated the power of this technology and established the theoretical foundation for binding studies. An FCCS experiment will yield the two autocorrelation curves of the single species and a cross-correlation curve. The codiffusing and hence bound fraction of molecules can then be extracted by simply determining the ratio of the $G(0)$ of the respective curves (G(cross)/G(auto)), assuming that the autocorrelation curves are free of cross-talk. If for example the concentration of a fluorescent ligand in binding assays to a labeled cellular receptor can be controlled, the bound fraction can be simply computed as above from $G(0)$ and used in standard Scatchard or Hill analysis to yield a K_d. Such analysis has been successfully applied for small-molecule ligands to transmembrane molecules in live cells[189,196–198] including neurons.[199] In assays involving two intracellular or even transmembrane components the situation is different since the difference in diffusion time, τ_c, yielded from the individual autocorrelation functions of the two components is often not high enough to complement the cross-correlation function, and so far only descriptive work has been published on the kinetics of protein–protein interaction, for example in the Fc−receptor complex during T-cell activation,[200] endocytosis of bacterial cholera toxin,[201] or EGF dimerization.[202] A major problem not solved so far is the requirement for long integration times (100 times the diffusion time) for slowly diffusing molecules dramati-

cally limiting the time resolution of kinetic analysis by FCCS. For transmembrane molecules at least 10 s, but sometimes up to 300 s, of correlation per time point is necessary.

9. Direct Assessment of Protein/Protein Interactions by FRET

9.1. Definition and Basic Properties

Förster resonance energy transfer (FRET) is the nonradiative transfer of energy between two fluorophores (called a donor and an acceptor) that have overlapping emission and absorption (excitation) spectra, respectively. This occurs when the two fluorophores are sufficiently close (2–8 nm range) and in a good orientation for efficient electromagnetic dipole–dipole interaction. Indeed, the FRET efficiency E is a steep function of the interaction distance R between the two molecules: $E = 1/[1 + (R/R_0)^6]$, where R_0 is the distance between donor and acceptor corresponding to $E = 50\%$. FRET measurement can therefore yield precise information about the proximity of two molecular species tagged with appropriate fluophores. When working with fluorescent proteins in live cells, the fact that the two fluophores need to be extremely close and properly oriented imposes strong constraints on the positioning of the fluorescent proteins in the two constructs by genetic engineering, and the correct folding and function of the tagged proteins have to be verified. Historically, the most commonly used pair of fluorescent proteins was CFP as donor and YFP as acceptor. However, with the engineering of new red fluorescent protein species,[24] several options are available and GFP and RFP are now being widely used as FRET partners. FRET can be measured by different approaches.[203]

A direct read-out is to excite the donor molecule and to measure the fluorescence emission of the acceptor molecule. Because the fluorescent proteins generally used for FRET have largely overlapping absorption and emission spectra, signals may bleed through standard fluorescence filters sets, and one needs to make the appropriate corrections (in particular measure donor and acceptor alone). The measurement of the full emission spectrum of the sample with acousto-optic tunable filters (AOTF) in a confocal microscope may provide better accuracy. This method is referred to as *spectral analysis*. One can indeed normalize the increase in fluorescence at the emission peak of the acceptor, by the decrease in fluorescence at the emission peak of the donor, to get a clean estimate of FRET efficiency. This approach has been applied to the actin-CFP/actin-YFP pair to show that during synaptic stimulation a fraction of actin at synapses switches from a monomeric form to a filamentous form, and conversely during synaptic depression.[132]

Another method relies on the selective photobleaching of the acceptor, using laser light at the maximum absorption wavelength.[204] Because the acceptor can no longer absorb energy otherwise transferred by the donor, acceptor photobleaching is accompanied by an increase in the fluorescence emitted by the donor. However, all these measurements are dependent on the relative amounts of the two molecules, which is not easy to control by standard transfection protocols. An alternative, but obviously a technical challenge, is to monitor FRET at the individual molecule level. For example, FRET was detected between the small G protein Ras fused with YFP (donor) and the fluorescent GTP analogue BodipyTR-GTP (acceptor) upon conditions of activation with epidermal growth factor, which also caused a reduction in Ras mobility, suggesting the formation of higher order complexes.[205] One can also detect the simultaneous presence of two single molecules at the same location,[206] but due to optical limitations, this type of measurement has a precision of at best 100 nm and cannot be taken as a proof that two proteins are interacting. Although also limited by optical resolution, the detection of FRET is an indicator that the two proteins are indeed interacting on the nanometer scale.

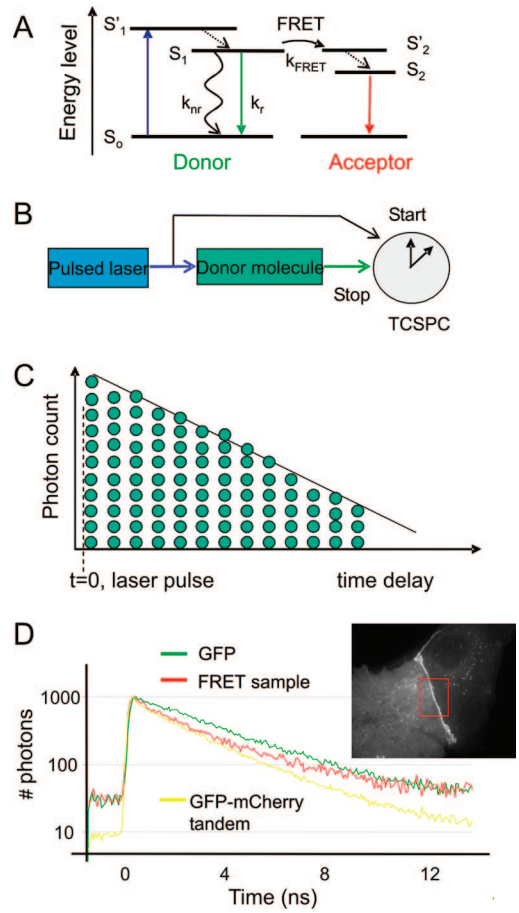

Figure 14. Measurement of FRET efficiency by FLIM. (A) Energy diagram showing the resting state (S_0) and excited states of the donor (S_1) and acceptor molecules (S_2). The donor fluorophore absorbs a photon (blue arrow) and can come back to the ground level by three independent processes: (1) nonradiative relaxation, with rate constant k_{nr}, (2) emission of a fluorescence photon (green arrow) at rate k_f, and (3) resonance energy transfer to an acceptor molecule (rate constant k_{FRET}), which reaches excited state S_2. The acceptor molecule can then emit a fluorescence photon of lower energy or higher wavelength (red arrow). (B) Scheme of the experimental setup to measure fluorescence lifetime using a pulsed laser and a time-correlated single-photon counter (TCSPC). (C) Log plot histogram of the time delays between laser pulse and photon emission. (D) Experimental curves obtained from COS cells expressing either N-cadherin-GFP alone (green curve), both N-cadherin-GFP and N-cadherin-RFP in adhesive junctions between glial cells (inset) enriched in N-cadherin (red), or a GFP-mCherry tandem as a positive control (a gift from M. Coppey's laboratory, Institut Jacques Monod, Paris). Histograms were obtained from approximately $10 \times 10\ \mu$m regions, and photons were accumulated for 10–30 s on a Leica SP2 confocal microscope equipped with a Becker-Hickl TCSPC board. Note that the GFP gives a single exponential ($\tau = 2.276$ ns), whereas GFP-mCherry is fitted by two exponential functions (30% $\tau_1 = 1.379$ ns; 70% $\tau_2 = 1.956$ ns, FRET efficiency = 30%), and so does the N-cadherin cotransfectant (40% $\tau_1 = 1.720$ ns; 60% $\tau_2 = 2.320$ ns; FRET efficiency = 26%), indicating *cis*-dimer formation between cadherins.

Table 2. Characteristics of the Various Optical Techniques[a]

category	optical tweezers	FRAP/ photoactivation	FCS/FCCS	SPT/SMT	FRET/FLIM
illumination	continuous IR laser + wide field fluorescence	1-P or 2-P continuous or pulsed, tuned to the absorption wavelength of the fluorophore	1-P or 2-P continuous or pulsed, confocal configuration	wide field (fluorescence or DIC) 2 colinear continuous lasers for photothermal	pulsed laser 1-P or 2-P
laser scanning	single or multiple fixed spots	fixed spot or scanning	fixed spot (parked beam)	NA/fixed spot, moving stage	scanning or wide field
detector	ICCD	ICCD or PMT	APD	ICCD/APD	TCSPC
readout	intensity changes	intensity changes	intensity fluctuations	2D trajectory	photon delay counts
analysis	fluorescence accumulation	fluorescence recovery after photobleaching	auto- and cross-correlation	mean-squared displacement	lifetime distribution
fitting	diffusion trap model	diffusion/reaction model	diffusion/ reaction + illumination profile	dwell time distributions, simulations	multiexponential
parameters	k_{on}	k_{off}, D	[C], D, k_{on}/k_{off}	D, k_{on}, k_{off} stoichiometry complete distributions	FRET efficiency, interaction distance

[a] Abbreviations: ICCD, intensified charge coupled device camera; APD, avalanche photodiode; PMT, photomultiplier tube; TCSPC, time-correlated single-photon counting; 1-P, one-photon illumination; 2-P, two-photon illumination; D, diffusion coefficient; C, concentration; k_{on}/k_{off}, reaction rate constants.

If fluorophores are excited with polarized light and the physical reorientation of the transition dipole (rotational diffusion in transmembrane molecules) is slower than the fluorescence lifetime, the emitted light will also be polarized. However, if an identical fluorophore is nearby, it may function as a FRET acceptor in what is called homo-FRET and then emit light that is not polarized in the same orientation anymore. The resulting loss in fluorescence anisotropy can be used as a measure of the interaction. The clustering of identical molecules can thus be observed, since any molecule can transfer energy to any other molecule, at a very low detectability level either at steady state[207] or time resolved.[208] This approach, which has allowed identification of microdomains of GPI-anchored proteins in the plasma membrane,[209] could also be used to analyze clustering of molecules in the postsynaptic density.

9.2. Fluorescence Lifetime Imaging (FLIM)

A nonambiguous estimation of the FRET efficiency can be made through fluorescence lifetime imaging (FLIM). The principle is to measure the time spent by the donor molecule in the excited state before emitting a photon by fluorescence[210] (Figure 14A). This duration is typically on the nanosecond time scale, e.g., 2.3 ns for GFP in live conditions, and independent of the brightness of the fluorophore. Because the de-excitation is a random event, it follows a Poisson process, and the distribution of lifetimes is usually a monoexponentially decreasing function characteristic of each fluorophore. Such measurement can be achieved in the time domain using a femtosecond pulsed laser (indifferently monophoton or two-photon) and time-correlated single-photon counting[211–213] (Figure 14B). The sample must be illuminated with low light levels so as to count at most one photon between two pulses of light (e.g., time interval of 12.5 ns at a 75 MHz pulse frequency). Otherwise, the detector could count photons from fluorophores that were excited at previous peaks, leading to underestimation of their lifetime.[214,215] This yields a histogram of the individual lifetimes, which can be fitted with multiexponential functions (Figure 14C). In confocal imaging, one can work pixel by pixel and integrate over long times, so as to obtain image maps of lifetimes that can reveal regional differences between different cellular subcompartments, as described in a study of the interaction between PSD-95 and potassium channels.[216] Alternatively, one can sum many pixels over a region of interest and work with faster time resolution and better fitting accuracy.

FRET is a process that can significantly alter the fluorescence lifetime of a fluorophore. Indeed, after absorbing a photon, excited donor molecules can go back to their relaxed state either through conventional fluorescence emission or by transferring their energy to acceptor molecules in a nonradiative fashion. Intuitively, one can consider that the subfraction of donor molecules that undergo FRET spend longer times in the excited state; therefore the fraction of fluorescence photons that are actually detected correspond to smaller lifetimes. Mathematically, the lifetime can be expressed as the inverse of the relaxation rate, which is the sum of individual rates from three different processes (nonradiative relaxation, fluorescence, and FRET); thus,

$$\tau = 1/(k_{nr} + k_f + k_{FRET}) \quad (8)$$

The presence of FRET (nonzero k_{FRET}) results in a specific reduction of the donor lifetime, and the FRET efficiency is calculated as $1 - \tau_{FRET}/\tau_{control}$, where $\tau_{control}$ is the lifetime of the donor alone and τ_{FRET} the lifetime in the presence of acceptor. The lifetime does not depend on the expression level of the donor molecule (e.g., in practice a 1 s acquisition on a very bright cell will yield exactly the same lifetime histogram as a 100 s acquisition on a cell expressing very low fluorescence levels). However, to get reproducible FRET values, the expression level of acceptor molecules has to match that of the donor. To this aim, one could choose cells that express saturating fluorescence levels of acceptor, but then one has to be careful about the presence of green signal from nonmature forms of red fluorescent proteins, which could contaminate donor emission. After doing all appropriate negative controls (donor alone, acceptor alone, or best donor + acceptor where fluorophores are far apart), the FRET efficiency can then be calculated by multiexponential fitting. In theory, these measurements yield a continuum of interaction distances and orientation angles that give rise to a series of exponential functions with many lifetimes. However, GFP and mRFP are good FRET partners in FLIM, because GFP alone shows monoexponential lifetime decay.[217] Then, with only two exponentials, the proportions of molecules that are interacting can be isolated and put in correspondence with

distinct biological populations (e.g., with the formation of well-identified clusters where the two molecules colocalize). We recently applied this technique to the study of the interaction between AMPA receptors and reported scaffold proteins. The results indicate rather weak interaction between GluR2-CFP and PICK-YFP and very strong interaction between stargazin-mCherry and PSD-95-GFP. For illustration, we show an example of FRET signals obtained between lateral N-cadherin dimers at cell junctions (Figure 14D).

10. Conclusion

We presented here a survey of the novel techniques in optical microscopy available to probe reactions between proteins at the plasma membrane, and more specifically within confined environments such as neuronal contacts. Each method has its own advantages and drawbacks, and it is generally advisable to combine several approaches, e.g., ensemble methods with single-molecule methods, to tackle the many facets of one biological problem (Table 2). Single-molecule approaches (SMT/SPT) provide an accurate detection of protein mobility with exquisite temporal and spatial resolutions, but the size of the probe particle leaves a problem of accessibility to restricted areas such as cell−cell junctions, extracellular matrix, or intracellular compartments. A major methodological breakthrough is needed from efforts in both chemistry and physics to design small enough derivatized particles that can diffuse without steric hindrance in thick biological tissues and be simultaneously detected by optical imaging. This would allow for example tracking the mobility of neurotransmitter receptors in acute brain slices whose physiological properties have been well worked out, e.g., in conditions of induced synaptic plasticity.

Ensemble methods based on average fluorescence intensities (e.g., FRAP) have limited temporal resolution and often assume a continuous and homogeneous medium, which is barely the case in cells even at the nanoscopic scale. Indeed, heterogeneities and multiple binding states are difficult to model and discriminate in a typical FRAP experiment. However, ensemble methods are relatively simple to implement, yield information rapidly, and have the major advantage of probing restricted cellular compartments. Although often heralded, the breakthrough of FCS and FCCS in cell biology as a versatile tool to provide real-time quantitative kinetic data on protein–protein interactions in live cells has not occurred yet. The complex behavior of molecules in live cells with very high time constants and the limited reservoir of labeled molecules render the use of this technology challenging. FRET/FLIM measurements provide a direct read-out of whether two proteins can assemble, but require time-consuming molecular biology work to make fluorescently tagged constructs that can functionally interact and require fine adjustments of the expression levels of the two proteins. Nevertheless, the design of new fluorescent proteins and more stable organic fluorophores, combined with novel laser sources and high-frequency operating light detectors, have allowed such techniques to shed light on the exquisite dynamics of many macromolecular assemblies at the cellular level. With no doubt, it is from concerted interdisciplinary efforts in cell biology, chemistry, and physics that more progress in this field will arise.

11. Acknowledgments

We thank C. Bats, C. Dequidt, X. Fournet, J. L. Pruvost, M. Renner, L. Mikasova, and E. Saint-Michel for image contributions and helpful discussions, C. Breillat, D. Bouchet, and B. Tessier for neuronal cultures, and P. Gonzales for technical assistance.We acknowledge funding from the Centre National de la Recherche Scientifique, the Conseil Régional d'Aquitaine, the Ministère de la Recherche, the Fondation pour la Recherche Médicale, The Human Frontier Science Program, the Association Française contre les Myopathies, ANR, and the European Community Grants QLG3-CT-2001-02089 and CT-2005-005320.

12. References

(1) Tessier-Lavigne, M. *Harvey Lect.* **2002**, *98*, 103.
(2) Garner, C. C.; Zhai, R. G.; Gundelfinger, E. D.; Ziv, N. E. *Trends Neurosci.* **2002**, *25*, 243.
(3) Garner, C. C.; Waites, C. L.; Ziv, N. E. *Cell Tissue Res.* **2006**, *326*, 249.
(4) Sudhof, T. C. *Annu. Rev. Neurosci.* **2004**, *27*, 509.
(5) Scannevin, R. H.; Huganir, R. L. *Nat. Rev. Neurosci.* **2000**, *1*, 133.
(6) Kim, E.; Sheng, M. *Nat. Rev. Neurosci.* **2004**, *5*, 771.
(7) Malenka, R. C.; Bear, M. F. *Neuron* **2004**, *44*, 5.
(8) Holtmaat, A. J.; Trachtenberg, J. T.; Wilbrecht, L.; Shepherd, G. M.; Zhang, X.; Knott, G. W.; Svoboda, K. *Neuron* **2005**, *45*, 279.
(9) Gray, N. W.; Weimer, R. M.; Bureau, I.; Svoboda, K. *PLoS Biol.* **2006**, *4*, e370.
(10) Tsuriel, S.; Geva, R.; Zamorano, P.; Dresbach, T.; Boeckers, T.; Gundelfinger, E. D.; Garner, C. C.; Ziv, N. E. *PLoS Biol.* **2006**, *4*, e271.
(11) Ziv, N. E.; Garner, C. C. *Nat. Rev. Neurosci.* **2004**, *5*, 385.
(12) Bresler, T.; Shapira, M.; Boeckers, T.; Dresbach, T.; Futter, M.; Garner, C. C.; Rosenblum, K.; Gundelfinger, E. D.; Ziv, N. E. *J. Neurosci.* **2004**, *24*, 1507.
(13) Holcman, D.; Triller, A. *Biophys. J.* **2006**, *91*, 2405.
(14) Shouval, H. Z. *Proc. Natl. Acad. Sci. U.S.A.* **2005**, *102*, 14440.
(15) Husi, H.; Grant, S. G. *Trends Neurosci.* **2001**, *24*, 259.
(16) Husi, H.; Ward, M. A.; Choudhary, J. S.; Blackstock, W. P.; Grant, S. G. *Nat. Neurosci.* **2000**, *3*, 661.
(17) Sheng, M.; Hoogenraad, C. C. *Annu. Rev. Biochem.* **2007**, *76*, 823.
(18) Cheng, D.; Hoogenraad, C. C.; Rush, J.; Ramm, E.; Schlager, M. A.; Duong, D. M.; Xu, P.; Wijayawardana, S. R.; Hanfelt, J.; Nakagawa, T.; Sheng, M.; Peng, J. *Mol. Cell. Proteomics* **2006**, *5*, 1158.
(19) Masugi-Tokita, M.; Shigemoto, R. *Curr. Opin. Neurobiol.* **2007**, *17*, 387.
(20) Cottrell, J. R.; Dube, G. R.; Egles, C.; Liu, G. *J. Neurophysiol.* **2000**, *84*, 1573.
(21) Momiyama, A.; Silver, R. A.; Hausser, M.; Notomi, T.; Wu, Y.; Shigemoto, R.; Cull-Candy, S. G. *J. Physiol.* **2003**, *549*, 75.
(22) Shimomura, O. *J. Microsc.* **2005**, *217*, 1.
(23) Stearns, T. *Curr. Biol.* **1995**, *5*, 262.
(24) Shaner, N. C.; Campbell, R. E.; Steinbach, P. A.; Giepmans, B. N.; Palmer, A. E.; Tsien, R. Y. *Nat. Biotechnol.* **2004**, *22*, 1567.
(25) Shaner, N. C.; Steinbach, P. A.; Tsien, R. Y. *Nat. Methods* **2005**, *2*, 905.
(26) Remington, S. J. *Curr. Opin. Struct. Biol.* **2006**, *16*, 714.
(27) Miesenbock, G.; De Angelis, D. A.; Rothman, J. E. *Nature* **1998**, *394*, 192.
(28) Hanson, G. T.; Aggeler, R.; Oglesbee, D.; Cannon, M.; Capaldi, R. A.; Tsien, R. Y.; Remington, S. J. *J. Biol. Chem.* **2004**, *279*, 13044.
(29) Bulina, M. E.; Lukyanov, K. A.; Britanova, O. V.; Onichtchouk, D.; Lukyanov, S.; Chudakov, D. M. *Nat. Protoc.* **2006**, *1*, 947.
(30) Lippincott-Schwartz, J.; Altan-Bonnet, N.; Patterson, G. H. *Nat. Cell Biol.* **2003**, *Suppl.*, S7.
(31) Lukyanov, K. A.; Chudakov, D. M.; Lukyanov, S.; Verkhusha, V. V. *Nat. Rev. Mol. Cell. Biol.* **2005**, *6*, 885.
(32) Patterson, G. H.; Lippincott-Schwartz, J. *Science* **2002**, *297*, 1873.
(33) Chudakov, D. M.; Verkhusha, V. V.; Staroverov, D. B.; Souslova, E. A.; Lukyanov, S.; Lukyanov, K. A. *Nat. Biotechnol.* **2004**, *22*, 1435.
(34) Washbourne, P.; McAllister, A. K. *Curr. Opin. Neurobiol.* **2002**, *12*, 566.
(35) Xia, Z.; Dudek, H.; Miranti, C. K.; Greenberg, M. E. *J. Neurosci.* **1996**, *16*, 5425.
(36) Yudowski, G. A.; Puthenveedu, M. A.; Leonoudakis, D.; Panicker, S.; Thorn, K. S.; Beattie, E. C.; von Zastrow, M. *J. Neurosci.* **2007**, *27*, 11112.
(37) Pelkmans, L.; Zerial, M. *Nature* **2005**, *436*, 128.
(38) Sugiyama, Y.; Kawabata, I.; Sobue, K.; Okabe, S. *Nat. Methods* **2005**, *2*, 677.
(39) Iino, R.; Koyama, I.; Kusumi, A. *Biophys. J.* **2001**, *80*, 2667.

(40) Harms, G. S.; Cognet, L.; Lommerse, P. H.; Blab, G. A.; Schmidt, T. *Biophys. J.* **2001**, *80*, 2396.
(41) Harms, G. S.; Cognet, L.; Lommerse, P. H.; Blab, G. A.; Kahr, H.; Gamsjager, R.; Spaink, H. P.; Soldatov, N. M.; Romanin, C.; Schmidt, T. *Biophys. J.* **2001**, *81*, 2639.
(42) Coussen, F.; Choquet, D.; Sheetz, M. P.; Erickson, H. P. *J. Cell Sci.* **2002**, *115*, 2581.
(43) Cognet, L.; Tardin, C.; Martin-Négrier, M. L.; Breillat, C.; Coussen, F.; Choquet, D.; Lounis, B. *J. Biomed. Optics* **2008**, *13* (3), in press.
(44) Ulbrich, M. H.; Isacoff, E. Y. *Nat. Methods* **2007**, *4*, 319.
(45) Kamiguchi, H.; Yoshihara, F. *J. Neurosci.* **2001**, *21*, 9194.
(46) Riehl, R.; Johnson, K.; Bradley, R.; Grunwald, G. B.; Cornel, E.; Lilienbaum, A.; Holt, C. E. *Neuron* **1996**, *17*, 837.
(47) Washbourne, P.; Dityatev, A.; Scheiffele, P.; Biederer, T.; Weiner, J. A.; Christopherson, K. S.; El-Husseini, A. *J. Neurosci.* **2004**, *24*, 9244.
(48) Okamura, K.; Tanaka, H.; Yagita, Y.; Saeki, Y.; Taguchi, A.; Hiraoka, Y.; Zeng, L. H.; Colman, D. R.; Miki, N. *J. Cell Biol.* **2004**, *167*, 961.
(49) Kamiguchi, H.; Hlavin, M. L.; Lemmon, V. *Mol. Cell. Neurosci.* **1998**, *12*, 48.
(50) Jamain, S.; Quach, H.; Betancur, C.; Rastam, M.; Colineaux, C.; Gillberg, I. C.; Soderstrom, H.; Giros, B.; Leboyer, M.; Gillberg, C.; Bourgeron, T. *Nat. Genet.* **2003**, *34*, 27.
(51) Tabuchi, K.; Blundell, J.; Etherton, M. R.; Hammer, R. E.; Liu, X.; Powell, C. M.; Sudhof, T. C. *Science* **2007**, *318*, 71.
(52) Pardo, C. A.; Eberhart, C. G. *Brain Pathol.* **2007**, *17*, 434.
(53) Nassoy, P. *Biophys. J.* **2007**, *93*, 361.
(54) Hukkanen, E. J.; Wieland, J. A.; Gewirth, A.; Leckband, D. E.; Braatz, R. D. *Biophys. J.* **2005**, *89*, 3434.
(55) Marshall, B. T.; Sarangapani, K. K.; Lou, J.; McEver, R. P.; Zhu, C. *Biophys. J.* **2005**, *88*, 1458.
(56) Chesla, S. E.; Selvaraj, P.; Zhu, C. *Biophys. J.* **1998**, *75*, 1553.
(57) Merkel, R.; Nassoy, P.; Leung, A.; Ritchie, K.; Evans, E. *Nature* **1999**, *397*, 50.
(58) Perret, E.; Benoliel, A. M.; Nassoy, P.; Pierres, A.; Delmas, V.; Thiery, J. P.; Bongrand, P.; Feracci, H. *EMBO J.* **2002**, *21*, 2537.
(59) Piper, J. W.; Swerlick, R. A.; Zhu, C. *Biophys. J.* **1998**, *74*, 492.
(60) Thoumine, O.; Kocian, P.; Kottelat, A.; Meister, J. J. *Eur. Biophys. J.* **2000**, *29*, 398.
(61) Stout, A. L. *Biophys. J.* **2001**, *80*, 2976.
(62) Zhu, C.; Long, M.; Chesla, S. E.; Bongrand, P. *Ann. Biomed. Eng.* **2002**, *30*, 305.
(63) Bell, G. I. *Science* **1978**, *200*, 618.
(64) Lauffenburger, D. A.; Linderman, J. J. *Receptors: Models for Binding, Trafficking, and Signaling*; Oxford University Press: New York, 1993.
(65) Dustin, M. L.; Bromley, S. K.; Davis, M. M.; Zhu, C. *Annu. Rev. Cell. Dev. Biol.* **2001**, *17*, 133.
(66) Pierres, A.; Benoliel, A. M.; Bongrand, P.; van der Merwe, P. A. *FEBS Lett.* **1997**, *403*, 239.
(67) Bayas, M. V.; Leung, A.; Evans, E.; Leckband, D. *Biophys. J.* **2006**, *90*, 1385.
(68) Chien, Y. H.; Jiang, N.; Li, F.; Zhang, F.; Zhu, C.; Leckband, D. *J. Biol. Chem.* **2008**, *283*, 1848.
(69) Zarnitsyna, V. I.; Huang, J.; Zhang, F.; Chien, Y. H.; Leckband, D.; Zhu, C. *Proc. Natl. Acad. Sci. U.S.A.* **2007**, *104*, 18037.
(70) Zhu, D. M.; Dustin, M. L.; Cairo, C. W.; Golan, D. E. *Biophys. J.* **2007**, *92*, 1022.
(71) Dustin, M. L.; Ferguson, L. M.; Chan, P. Y.; Springer, T. A.; Golan, D. E. *J. Cell Biol.* **1996**, *132*, 465.
(72) Dustin, M. L.; Golan, D. E.; Zhu, D. M.; Miller, J. M.; Meier, W.; Davies, E. A.; van der Merwe, P. A. *J. Biol. Chem.* **1997**, *272*, 30889.
(73) Dustin, M. L. *J. Biol. Chem.* **1997**, *272*, 15782.
(74) Grakoui, A.; Bromley, S. K.; Sumen, C.; Davis, M. M.; Shaw, A. S.; Allen, P. M.; Dustin, M. L. *Science* **1999**, *285*, 221.
(75) Lee, S. J.; Hori, Y.; Groves, J. T.; Dustin, M. L.; Chakraborty, A. K. *Trends Immunol.* **2002**, *23*, 500.
(76) Lee, S. J.; Hori, Y.; Groves, J. T.; Dustin, M. L.; Chakraborty, A. K. *Trends Immunol.* **2002**, *23*, 492.
(77) Axelrod, D.; Burghardt, T. P.; Thompson, N. L. *Annu. Rev. Biophys. Bioeng.* **1984**, *13*, 247.
(78) Lang, T.; Wacker, I.; Steyer, J.; Kaether, C.; Wunderlich, I.; Soldati, T.; Gerdes, H. H.; Almers, W. *Neuron* **1997**, *18*, 857.
(79) Douglass, A. D.; Vale, R. D. *Cell* **2005**, *121*, 937.
(80) Dustin, M. L.; Colman, D. R. *Science* **2002**, *298*, 785.
(81) Pautot, S.; Lee, H.; Isacoff, E. Y.; Groves, J. T. *Nat. Chem. Biol.* **2005**, *1*, 283.
(82) Baksh, M. M.; Dean, C.; Pautot, S.; Demaria, S.; Isacoff, E.; Groves, J. T. *Langmuir* **2005**, *21*, 10693.
(83) Scheiffele, P.; Fan, J.; Choih, J.; Fetter, R.; Serafini, T. *Cell* **2000**, *101*, 657.
(84) Groves, J. T.; Dustin, M. L. *J. Immunol. Methods* **2003**, *278*, 19.
(85) Dean, C.; Scholl, F. G.; Choih, J.; DeMaria, S.; Berger, J.; Isacoff, E.; Scheiffele, P. *Nat. Neurosci.* **2003**, *6*, 708.
(86) Ashkin, A. *Proc. Natl. Acad. Sci. U.S.A.* **1997**, *94*, 4853.
(87) Thoumine, O.; Saint-Michel, E.; Dequidt, C.; Falk, J.; Rudge, R.; Galli, T.; Faivre-Sarrailh, C.; Choquet, D. *Biophys. J.* **2005**, *89*, L40.
(88) Thoumine, O.; Meister, J. J. *J. Theor. Biol.* **2000**, *204*, 381.
(89) Dequidt, C.; Danglot, L.; Alberts, P.; Galli, T.; Choquet, D.; Thoumine, O. *Mol. Biol. Cell* **2007**, *18*, 3131.
(90) Garver, T. D.; Ren, Q.; Tuvia, S.; Bennett, V. *J. Cell Biol.* **1997**, *137*, 703.
(91) Gil, O. D.; Sakurai, T.; Bradley, A. E.; Fink, M. Y.; Cassella, M. R.; Kuo, J. A.; Felsenfeld, D. P. *J. Cell Biol.* **2003**, *162*, 719.
(92) Kamiguchi, H.; Lemmon, V. *J. Neurosci.* **2000**, *20*, 3676.
(93) Baumgartner, W.; Hinterdorfer, P.; Ness, W.; Raab, A.; Vestweber, D.; Schindler, H.; Drenckhahn, D. *Proc. Natl. Acad. Sci. U.S.A.* **2000**, *97*, 4005.
(94) Alon, R.; Hammer, D. A.; Springer, T. A. *Nature* **1995**, *374*, 539.
(95) Sivasankar, S.; Gumbiner, B.; Leckband, D. *Biophys. J.* **2001**, *80*, 1758.
(96) Perret, E.; Leung, A.; Feracci, H.; Evans, E. *Proc. Natl. Acad. Sci. U.S.A.* **2004**, *101*, 16472.
(97) Marshall, B. T.; Long, M.; Piper, J. W.; Yago, T.; McEver, R. P.; Zhu, C. *Nature* **2003**, *423*, 190.
(98) Pierres, A.; Benoliel, A. M.; Bongrand, P.; van der Merwe, P. A. *Proc. Natl. Acad. Sci. U.S.A.* **1996**, *93*, 15114.
(99) Evans, E.; Leung, A.; Heinrich, V.; Zhu, C. *Proc. Natl. Acad. Sci. U.S.A.* **2004**, *101*, 11281.
(100) Breillat, C.; Thoumine, O.; Choquet, D. *Biochem. Biophys. Res. Commun.* **2007**, *359*, 655.
(101) Troyanovsky, R. B.; Sokolov, E.; Troyanovsky, S. M. *Mol. Cell. Biol.* **2003**, *23*, 7965.
(102) Brummendorf, T.; Lemmon, V. *Curr. Opin. Cell Biol.* **2001**, *13*, 611.
(103) Baumgartner, W.; Schutz, G. J.; Wiegand, J.; Golenhofen, N.; Drenckhahn, D. *J. Cell Sci.* **2003**, *116*, 1001.
(104) Fogel, A. I.; Akins, M. R.; Krupp, A. J.; Stagi, M.; Stein, V.; Biederer, T. *J. Neurosci.* **2007**, *27*, 12516.
(105) Axelrod, D.; Koppel, D. E.; Schlessinger, J.; Elson, E.; Webb, W. W. *Biophys. J.* **1976**, *16*, 1055.
(106) Edidin, M.; Stroynowski, I. *J. Cell Biol.* **1991**, *112*, 1143.
(107) Kenworthy, A. K.; Nichols, B. J.; Remmert, C. L.; Hendrix, G. M.; Kumar, M.; Zimmerberg, J.; Lippincott-Schwartz, J. *J. Cell Biol.* **2004**, *165*, 735.
(108) Feder, T. J.; Brust-Mascher, I.; Slattery, J. P.; Baird, B.; Webb, W. W. *Biophys. J.* **1996**, *70*, 2767.
(109) Sprague, B. L.; Pego, R. L.; Stavreva, D. A.; McNally, J. G. *Biophys. J.* **2004**, *86*, 3473.
(110) Crank, J. *The Mathematics of Diffusion;* Oxford University Press: New York, 1975.
(111) Thoumine, O.; Lambert, M.; Mege, R. M.; Choquet, D. *Mol. Biol. Cell* **2006**, *17*, 862.
(112) Ballestrem, C.; Hinz, B.; Imhof, B. A.; Wehrle-Haller, B. *J. Cell Biol.* **2001**, *155*, 1319.
(113) Wehrle-Haller, B. *Methods Mol. Biol.* **2007**, *370*, 173.
(114) Hollmann, M.; Heinemann, S. *Annu. Rev. Neurosci.* **1994**, *17*, 31.
(115) Chen, L.; Chetkovich, D. M.; Petralia, R. S.; Sweeney, N. T.; Kawasaki, Y.; Wenthold, R. J.; Bredt, D. S.; Nicoll, R. A. *Nature* **2000**, *408*, 936.
(116) Schnell, E.; Sizemore, M.; Karimzadegan, S.; Chen, L.; Bredt, D. S.; Nicoll, R. A. *Proc. Natl. Acad. Sci. U.S.A.* **2002**, *99*, 13902.
(117) Ashby, M. C.; Ibaraki, K.; Henley, J. M. *Trends Neurosci.* **2004**, *27*, 257.
(118) Bloodgood, B. L.; Sabatini, B. L. *Science* **2005**, *310*, 866.
(119) Richards, D. A.; De Paola, V.; Caroni, P.; Gahwiler, B. H.; McKinney, R. A. *J. Physiol.* **2004**, *558*, 503.
(120) Schuss, Z.; Singer, A.; Holcman, D. *Proc. Natl. Acad. Sci. U.S.A.* **2007**, *104*, 16098.
(121) Adesnik, H.; Nicoll, R. A.; England, P. M. *Neuron* **2005**, *48*, 977.
(122) Tovar, K. R.; Westbrook, G. L. *Neuron* **2002**, *34*, 255.
(123) Thomas, P.; Mortensen, M.; Hosie, A. M.; Smart, T. G. *Nat. Neurosci.* **2005**, *8*, 889.
(124) Li, Z.; Sheng, M. *Nat. Rev. Mol. Cell. Biol.* **2003**, *4*, 833.
(125) Sytnyk, V.; Leshchyns'ka, I.; Delling, M.; Dityateva, G.; Dityatev, A.; Schachner, M. *J. Cell Biol.* **2002**, *159*, 649.
(126) Horton, A. C.; Racz, B.; Monson, E. E.; Lin, A. L.; Weinberg, R. J.; Ehlers, M. D. *Neuron* **2005**, *48*, 757.
(127) Lu, J.; Helton, T. D.; Blanpied, T. A.; Racz, B.; Newpher, T. M.; Weinberg, R. J.; Ehlers, M. D. *Neuron* **2007**, *55*, 874.
(128) Passafaro, M.; Piech, V.; Sheng, M. *Nat. Neurosci.* **2001**, *4*, 917.
(129) Park, M.; Salgado, J. M.; Ostroff, L.; Helton, T. D.; Robinson, C. G.; Harris, K. M.; Ehlers, M. D. *Neuron* **2006**, *52*, 817.
(130) Kennedy, M. J.; Ehlers, M. D. *Annu. Rev. Neurosci.* **2006**, *29*, 325.
(131) Star, E. N.; Kwiatkowski, D. J.; Murthy, V. N. *Nat. Neurosci.* **2002**, *5*, 239.

(132) Okamoto, K.; Nagai, T.; Miyawaki, A.; Hayashi, Y. *Nat. Neurosci.* **2004**, *7*, 1104.
(133) Colicos, M. A.; Collins, B. E.; Sailor, M. J.; Goda, Y. *Cell* **2001**, *107*, 605.
(134) Sharma, K.; Fong, D. K.; Craig, A. M. *Mol. Cell. Neurosci.* **2006**, *31*, 702.
(135) Murase, S.; Mosser, E.; Schuman, E. M. *Neuron* **2002**, *35*, 91.
(136) Tai, C. Y.; Mysore, S. P.; Chiu, C.; Schuman, E. M. *Neuron* **2007**, *54*, 771.
(137) Yamada, S.; Pokutta, S.; Drees, F.; Weis, W. I.; Nelson, W. J. *Cell* **2005**, *123*, 889.
(138) Kuriu, T.; Inoue, A.; Bito, H.; Sobue, K.; Okabe, S. *J. Neurosci.* **2006**, *26*, 7693.
(139) Ashby, M. C.; Maier, S. R.; Nishimune, A.; Henley, J. M. *J. Neurosci.* **2006**, *26*, 7046.
(140) Rasse, T. M.; Fouquet, W.; Schmid, A.; Kittel, R. J.; Mertel, S.; Sigrist, C. B.; Schmidt, M.; Guzman, A.; Merino, C.; Qin, G.; Quentin, C.; Madeo, F. F.; Heckmann, M.; Sigrist, S. J. *Nat. Neurosci.* **2005**, *8*, 898.
(141) Kummer, T. T.; Misgeld, T.; Sanes, J. R. *Curr. Opin. Neurobiol.* **2006**, *16*, 74.
(142) Bruneau, E. G.; Macpherson, P. C.; Goldman, D.; Hume, R. I.; Akaaboune, M. *Dev. Biol.* **2005**, *288*, 248.
(143) Sekine-Aizawa, Y.; Huganir, R. L. *Proc. Natl. Acad. Sci. U.S.A.* **2004**, *101*, 17114.
(144) Chen, I.; Ting, A. Y. *Curr. Opin. Biotechnol.* **2005**, *16*, 35.
(145) Howarth, M.; Takao, K.; Hayashi, Y.; Ting, A. Y. *Proc. Natl. Acad. Sci. U.S.A.* **2005**, *102*, 7583.
(146) Borgdorff, A. J.; Choquet, D. *Nature* **2002**, *417*, 649.
(147) Tardin, C.; Cognet, L.; Bats, C.; Lounis, B.; Choquet, D. *EMBO J.* **2003**, *22*, 4656.
(148) Groc, L.; Heine, M.; Cognet, L.; Brickley, K.; Stephenson, F. A.; Lounis, B.; Choquet, D. *Nat. Neurosci.* **2004**, *7*, 695.
(149) Groc, L.; Lafourcade, M.; Heine, M.; Renner, M.; Racine, V.; Sibarita, J. B.; Lounis, B.; Choquet, D.; Cognet, L. *J. Neurosci.* **2007**, *27*, 12433.
(150) Dubertret, B.; Skourides, P.; Norris, D. J.; Noireaux, V.; Brivanlou, A. H.; Libchaber, A. *Science* **2002**, *298*, 1759.
(151) Larson, D. R.; Zipfel, W. R.; Williams, R. M.; Clark, S. W.; Bruchez, M. P.; Wise, F. W.; Webb, W. W. *Science* **2003**, *300*, 1434.
(152) Dahan, M.; Levi, S.; Luccardini, C.; Rostaing, P.; Riveau, B.; Triller, A. *Science* **2003**, *302*, 442.
(153) Groc, L.; Heine, M.; Cousins, S. L.; Stephenson, F. A.; Lounis, B.; Cognet, L.; Choquet, D. *Proc. Natl. Acad. Sci. U.S.A.* **2006**, *103*, 18769.
(154) Boyer, D.; Tamarat, P.; Maali, A.; Lounis, B.; Orrit, M. *Science* **2002**, *297*, 1160.
(155) Cognet, L.; Tardin, C.; Boyer, D.; Choquet, D.; Tamarat, P.; Lounis, B. *Proc. Natl. Acad. Sci. U.S.A.* **2003**, *100*, 11350.
(156) Berciaud, S.; Cognet, L.; Blab, G. A.; Lounis, B. *Phys. Rev. Lett.* **2004**, *93*, 257402.
(157) Lasne, D.; Blab, G. A.; Berciaud, S.; Heine, M.; Groc, L.; Choquet, D.; Cognet, L.; Lounis, B. *Biophys. J.* **2006**, *91*, 4598.
(158) Hancock, J. F. *Nat. Rev. Mol. Cell. Biol.* **2006**, *7*, 456.
(159) Kusumi, A.; Nakada, C.; Ritchie, K.; Murase, K.; Suzuki, K.; Murakoshi, H.; Kasai, R. S.; Kondo, J.; Fujiwara, T. *Annu. Rev. Biophys. Biomol. Struct.* **2005**, *34*, 351.
(160) Simson, R.; Yang, B.; Moore, S. E.; Doherty, P.; Walsh, F. S.; Jacobson, K. A. *Biophys. J.* **1998**, *74*, 297.
(161) Saxton, M. J.; Jacobson, K. *Annu. Rev. Biophys. Biomol. Struct.* **1997**, *26*, 373.
(162) Suzuki, K. G.; Fujiwara, T. K.; Edidin, M.; Kusumi, A. *J. Cell Biol.* **2007**, *177*, 731.
(163) Suzuki, K. G.; Fujiwara, T. K.; Sanematsu, F.; Iino, R.; Edidin, M.; Kusumi, A. *J. Cell Biol.* **2007**, *177*, 717.
(164) Qian, H.; Sheetz, M. P.; Elson, E. L. *Biophys. J.* **1991**, *60*, 910.
(165) Simson, R.; Sheets, E. D.; Jacobson, K. *Biophys. J.* **1995**, *69*, 989.
(166) Meier, J.; Vannier, C.; Serge, A.; Triller, A.; Choquet, D. *Nat. Neurosci.* **2001**, *4*, 253.
(167) Serge, A.; Fourgeaud, L.; Hemar, A.; Choquet, D. *J. Neurosci.* **2002**, *22*, 3910.
(168) Bats, C.; Groc, L.; Choquet, D. *Neuron* **2007**, *53*, 719.
(169) Ehrensperger, M. V.; Hanus, C.; Vannier, C.; Triller, A.; Dahan, M. *Biophys. J.* **2007**, *92*, 3706.
(170) Schwille, P.; Kummer, S.; Heikal, A. A.; Moerner, W. E.; Webb, W. W. *Proc. Natl. Acad. Sci. U.S.A.* **2000**, *97*, 151.
(171) Schwille, P.; Haupts, U.; Maiti, S.; Webb, W. W. *Biophys. J.* **1999**, *77*, 2251.
(172) Haustein, E.; Schwille, P. *Annu. Rev. Biophys. Biomol. Struct.* **2007**, *36*, 151.
(173) Kim, S. A.; Heinze, K. G.; Schwille, P. *Nat. Methods* **2007**, *4*, 963.
(174) Wawrezinieck, L.; Rigneault, H.; Marguet, D.; Lenne, P. F. *Biophys. J.* **2005**, *89*, 4029.
(175) Lenne, P. F.; Wawrezinieck, L.; Conchonaud, F.; Wurtz, O.; Boned, A.; Guo, X. J.; Rigneault, H.; He, H. T.; Marguet, D. *EMBO J.* **2006**, *25*, 3245.
(176) Mainen, Z. F.; Maletic-Savatic, M.; Shi, S. H.; Hayashi, Y.; Malinow, R.; Svoboda, K. *Methods* **1999**, *18*, 231.
(177) Sobczyk, A.; Svoboda, K. *Neuron* **2007**, *53*, 17.
(178) Matsuzaki, M.; Ellis-Davies, G. C.; Nemoto, T.; Miyashita, Y.; Iino, M.; Kasai, H. *Nat. Neurosci.* **2001**, *4*, 1086.
(179) Bloodgood, B. L.; Sabatini, B. L. *Neuron* **2007**, *53*, 249.
(180) Levene, M. J.; Korlach, J.; Turner, S. W.; Foquet, M.; Craighead, H. G.; Webb, W. W. *Science* **2003**, *299*, 682.
(181) Samiee, K. T.; Moran-Mirabal, J. M.; Cheung, Y. K.; Craighead, H. G. *Biophys. J.* **2006**, *90*, 3288.
(182) Wenger, J.; Conchonaud, F.; Dintinger, J.; Wawrezinieck, L.; Ebbesen, T. W.; Rigneault, H.; Marguet, D.; Lenne, P. F. *Biophys. J.* **2007**, *92*, 913.
(183) Willig, K. I.; Harke, B.; Medda, R.; Hell, S. W. *Nat. Methods* **2007**, *4*, 915.
(184) Willig, K. I.; Kellner, R. R.; Medda, R.; Hein, B.; Jakobs, S.; Hell, S. W. *Nat. Methods* **2006**, *3*, 721.
(185) Klar, T. A.; Jakobs, S.; Dyba, M.; Egner, A.; Hell, S. W. *Proc. Natl. Acad. Sci. U.S.A.* **2000**, *97*, 8206.
(186) Kastrup, L.; Blom, H.; Eggeling, C.; Hell, S. W. *Phys. Rev. Lett.* **2005**, *94*, 178104.
(187) Thompson, N. L.; Steele, B. L. *Nat. Protoc.* **2007**, *2*, 878.
(188) Lieto, A. M.; Cush, R. C.; Thompson, N. L. *Biophys. J.* **2003**, *85*, 3294.
(189) Politz, J. C.; Browne, E. S.; Wolf, D. E.; Pederson, T. *Proc. Natl. Acad. Sci. U.S.A.* **1998**, *95*, 6043.
(190) Chen, Y.; Muller, J. D.; So, P. T.; Gratton, E. *Biophys. J.* **1999**, *77*, 553.
(191) Chen, Y.; Muller, J. D.; Ruan, Q.; Gratton, E. *Biophys. J.* **2002**, *82*, 133.
(192) Muller, J. D.; Chen, Y.; Gratton, E. *Biophys. J.* **2000**, *78*, 474.
(193) Schluter, O. M.; Xu, W.; Malenka, R. C. *Neuron* **2006**, *51*, 99.
(194) Bacia, K.; Schwille, P. *Nat. Protoc.* **2007**, *2*, 2842.
(195) Kogure, T.; Karasawa, S.; Araki, T.; Saito, K.; Kinjo, M.; Miyawaki, A. *Nat. Biotechnol.* **2006**, *24*, 577.
(196) Briddon, S. J.; Middleton, R. J.; Cordeaux, Y.; Flavin, F. M.; Weinstein, J. A.; George, M. W.; Kellam, B.; Hill, S. J. *Proc. Natl. Acad. Sci. U.S.A.* **2004**, *101*, 4673.
(197) Hegener, O.; Prenner, L.; Runkel, F.; Baader, S. L.; Kappler, J.; Haberlein, H. *Biochemistry* **2004**, *43*, 6190.
(198) Schwartz, J. W.; Novarino, G.; Piston, D. W.; DeFelice, L. J. *J. Biol. Chem.* **2005**, *280*, 19177.
(199) Meissner, O.; Haberlein, H. *Biochemistry* **2003**, *42*, 1667.
(200) Larson, D. R.; Gosse, J. A.; Holowka, D. A.; Baird, B. A.; Webb, W. W. *J. Cell Biol.* **2005**, *171*, 527.
(201) Bacia, K.; Majoul, I. V.; Schwille, P. *Biophys. J.* **2002**, *83*, 1184.
(202) Liu, P.; Sudhaharan, T.; Koh, R. M.; Hwang, L. C.; Ahmed, S.; Maruyama, I. N.; Wohland, T. *Biophys. J.* **2007**, *93*, 684.
(203) Elangovan, M.; Day, R. N.; Periasamy, A. *J. Microsc.* **2002**, *205*, 3.
(204) Gadella, T. W., Jr.; Jovin, T. M *J. Cell Biol.* **1995**, *129*, 1543.
(205) Murakoshi, H.; Iino, R.; Kobayashi, T.; Fujiwara, T.; Ohshima, C.; Yoshimura, A.; Kusumi, A. *Proc. Natl. Acad. Sci. U.S.A.* **2004**, *101*, 7317.
(206) Koyama-Honda, I.; Ritchie, K.; Fujiwara, T.; Iino, R.; Murakoshi, H.; Kasai, R. S.; Kusumi, A. *Biophys. J.* **2005**, *88*, 2126.
(207) Varma, R.; Mayor, S. *Nature* **1998**, *394*, 798.
(208) Sharma, P.; Varma, R.; Sarasij, R. C.; Ira; Gousset, K.; Krishnamoorthy, G.; Rao, M.; Mayor, S. *Cell* **2004**, *116*, 577.
(209) Rao, M.; Mayor, S. *Biochim. Biophys. Acta* **2005**, *1746*, 221.
(210) Bastiaens, P. I.; Squire, A. *Trends Cell. Biol.* **1999**, *9*, 48.
(211) Harpur, A. G.; Wouters, F. S.; Bastiaens, P. I. *Nat. Biotechnol.* **2001**, *19*, 167.
(212) Tramier, M.; Gautier, I.; Piolot, T.; Ravalet, S.; Kemnitz, K.; Coppey, J.; Durieux, C.; Mignotte, V.; Coppey-Moisan, M. *Biophys. J.* **2002**, *83*, 3570.
(213) Tramier, M.; Piolot, T.; Gautier, I.; Mignotte, V.; Coppey, J.; Kemnitz, K.; Durieux, C.; Coppey-Moisan, M. *Methods Enzymol.* **2003**, *360*, 580.
(214) Spriet, C.; Trinel, D.; Waharte, F.; Deslee, D.; Vandenbunder, B.; Barbillat, J.; Heliot, L. *Microsc. Res. Tech.* **2007**, *70*, 85.
(215) Waharte, F.; Spriet, C.; Heliot, L. *Cytometry A* **2006**, *69*, 299.
(216) Biskup, C.; Kelbauskas, L.; Zimmer, T.; Benndorf, K.; Bergmann, A.; Becker, W.; Ruppersberg, J. P.; Stockklausner, C.; Klocker, N. *J. Biomed. Opt.* **2004**, *9*, 753.
(217) Tramier, M.; Zahid, M.; Mevel, J. C.; Masse, M. J.; Coppey-Moisan, M. *Microsc. Res. Tech.* **2006**, *69*, 933.
(218) Yan, Y.; Broadie, K. *J. Neurosci. Methods* **2007**, *162*, 198.
(219) Schmidt, C. E.; Chen, T.; Lauffenburger, D. A. *Biophys. J.* **1994**, *67*, 461.

CR078204M